BRNO UNIVERSITY OF TECHNOLOGY
VYSOKÉ UČENÍ TECHNICKÉ V BRNĚ

CENTRAL EUROPEAN INSTITUTE OF TECHNOLOGY BUT
STŘEDOEVROPSKÝ TECHNOLOGICKÝ INSTITUT VUT

MAGNETICALLY ASSEMBLED NANOPARTICLE STRUCTURES AND THEIR EFFECT ON MECHANICAL RESPONSE OF POLYMER NANOCOMPOSITES

MAGNETICKY USPOŘÁDANÉ STRUKTURY V POLYMERNÍCH NANOKOMPOZITECH A JEJICH VLIV NA MECHANICKOU ODEZVU

DOCTORAL THESIS
DIZERTAČNÍ PRÁCE

AUTHOR — **Ing. Marek Zbončák**
AUTOR PRÁCE

SUPERVISOR — **prof. RNDr. Josef Jančář, CSc.**
ŠKOLITEL

BRNO 2018

Bibliographic citation of dissertation thesis:

ZBONČÁK, M. *Magneticky uspořádané struktury v polymerních nanokompozitech a jejich vliv na mechanickou odezvu.* Brno: Vysoké učení technické v Brně, Středoevropský technologický institut VUT, 2018. 110 s. Vedoucí dizertační práce prof. RNDr. Josef Jančář, CSc..

……..
Signature of author

List of Contents

Abstract

Magnetically directed self-assembly in polymer nanocomposites is studied in this dissertation thesis. Structuring of the polymer nanocomposites by application of relatively weak external magnetic fields (B=0-50 mT) has been proven to be convenient method for the control of their nano- and microstructure. The effect of the field strength, particle loading, viscosity and assembling time on the resulted structure was studied in different systems such as photopolymer, polyurethane or colloidally dispersed magnetic nanoparticles in acetone with a small amount of dissolved polymer. Self-assembled structures – without application of the external magnetic field exhibit a multi-step aggregation into nanoparticle assemblies with a complex shape. By the calculation of interaction energies between the nanoparticles, magnetic interactions were attributed to be mainly responsible for the aggregation in self-assembled systems. With an increasing magnetic field, magnetic nanoparticles are rapidly arranged into high aspect ratio one-dimensional particle chains with a homogenous orientation in the bulk polymer matrix. After prolonged assembling time, the structures gradually grow from small submicro structures to large microscopic superstructures. This method exhibits large potential to be used for controlled creation of wide variety of structures in polymer nanocomposites suitable for technological applications and/or for fundamental studies. Magnetically structured polymer nanocomposites show significant directional anisotropy of composite's stiffness at the temperatures above glass transition of the system while there is no effect on the mechanical response in glassy state. Longitudinally oriented structures exhibit much stronger effect on the composite's stiffness. Reinforcing effectivity exhibits temperature dependent course with a maximum obtained approximately 60 °C above glass transition. The structure of magnetically assembled polymer nanocomposites was described by multi-level hierarchic model of material. Micromechanics was used to address the orientation dependent reinforcement and temperature dependent stiffness of the hybrid nanoparticle-polymer structures. Load carrying capability, deformation and non-zero stiffness of the hybrid structures were attributed to be responsible for the reinforcement of the polymer nanocomposites. The presence of polymer bridges between nanoparticles transmitting the stress through the magnetic structures is proposed to be essential for the mechanical properties of polymer nanocomposites and for stiffness of the hybrid structures.

Keywords: Polymer nanocomposites, Self-assembly, Magnetic directed self-assembly, Bottom-up assembly, Aggregation, Magnetic interaction, Thermo-mechanical properties, Anisotropy, Multi-level hierarchy, Polymer immobilization, Structure-property relationships

Abstrakt

Magneticky řízené samo-uspořádávání v polymerních nanokompozitech je studováno v této dizertační práci. Strukturování polymerních nanokompozitů pomocí relativně slabých magnetických polí (B=0-50 mT) bylo prokázáno jako praktická metoda pro kontrolu jejích nano a mikrostruktury. Vliv intenzity magnetického pole, množství nanočástic, viskozity a času uspořádávání na výslednou strukturu byl studován v různých systémech jako fotopolymer, polyuretan nebo koloidně dispergované nanočástice v acetonu s malým množstvím rozpuštěného polymeru. Samo-uspořádané struktury – bez aplikace vnějšího magnetického pole vykazují vícekrokovou agregaci nanočástic do uskupení s komplexním tvarem. Magnetické interakce byly označené jako odpovědné za agregaci nanočástic v samo-uspořádaných systémech pomocí výpočtů energii mezi-částicových interakcí. S rostoucím magnetickým polem, magnetické nanočástice jsou rychle uspořádané do jednorozměrných částicových řetězů s vysokým aspektním poměrem a homogenní orientaci v polymerní matrici. S prodluženým časem uspořádaní, tyto struktury postupně rostou z malých submikrometrových struktur do velkých mikroskopických super struktur. Táto metoda vykazuje velký potenciál pro kontrolovanou přípravu široké škály struktur v polymerních nanokompozitech vhodných pro technologické aplikace a také pro fundamentální studie. Magneticky uspořádané polymerní nanokompozity vykazují značnou směrovou anisotropii tuhosti kompozitu nad jeho skelným přechodem přičemž, pod skelným přechodem systému není pozorován žádný efekt. Podélně orientované struktury vykazují větší příspěvek k tuhosti kompozitů. Efektivnost vyztužení vykazuje teplotně závislý průběh a maximum je pozorováno přibližně 60 °C nad skelným přechodem. Struktura magneticky uspořádaného polymerního nanokompozitu byla popsána vícero-úrovňovým hierarchickým modelem materiálu. Mikromechanika byla využitá k popisu směrově závislého vyztužení polymerních nanokompozitů a k popisu teplotně závislé tuhosti hybridních struktur složených z nanočástic a polymeru. Schopnost nést napětí, deformovat se a nenulová tuhost hybridních struktur je odpovědná za vyztužení polymerních nanokompozitů. Přítomnost polymerních přemostění mezi nanočásticemi, které přenášejí napěti skrze magnetické struktury je označená jako nezbytná pro mechanickou odezvu polymerních nanokompozitů a pro tuhost hybridních struktur.

Klíčové slova: Polymerní nanokompozity, Samo-uspořádávání, Magneticky řízené samo-uspořádávání, Bottom-up uspořádávání, Agregace, Magnetická interakce, Termo-mechanické vlastností, Anisotropie, Více úrovňová hierarchie, Imobilizace polymeru, Vztah mezi strukturou a vlastnostmi

1 Introduction

1.1 Magnetically directed self-assembly in polymer composites

Despite relentless attempts of researchers to achieve the control over the assembling of the nanoparticles (NPs) in polymer matrix, common isotropic particle assemblies are typical output of their efforts – dispersion, clusters, aggregates. Compared to self-assembly techniques which are most commonly employed for polymer nanocomposites (PNCs) preparation, magnetic directed self-assembly can produce various anisotropic structures with a conveniently controlled and homogenous orientation (see Figure 1). Therefore, it is not surprise that this technique found its place among the processing protocols for PNCs. Individual MNP represent a magnetic dipole consisted from the north and south pole and adjacent magnetic dipoles interact with each other via their magnetic fields and assemble into complex anisotropic structures (*1*). The resulted structure depends on multiple processing parameters such as strength, shape and gradient of magnetic field, particle concentration and inter particle distance, magnetic response of the particles, viscosity of environment or assembling time (*2-12*).

For the fabrication of magnetically assembled PNCs, various laboratory scale processing techniques have been used by researchers. Methods such as solution casting of thin films (*13-17*), bulk *in-situ* thermal (*18-28*) or photo (*29-31*) polymerization during magnetic irradiation of the samples are most frequently used.

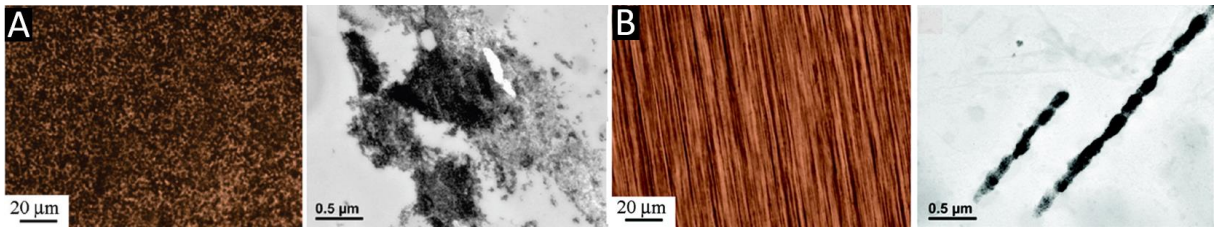

Figure 1 Optical and TEM images of (A) self-assembled and (B) magnetically assembled structure of γ-Fe_2O_3/PEMMA polymer nanocomposite. Reprinted with permission from ref. (*14*). Copyright 2011 American Chemical Society.

1.2 Thermo-mechanical properties of polymer nanocomposites

Addition of NPs into polymer matrix results in non-trivial enhancement of macroscopic thermo-mechanical response. Classic composite micromechanics theories which are quite viable to explain the mechanical response of micro composites fail in the case of polymer nanocomposites. There is a large unexplored gap in the knowledge leading to the connection of nanoscopic mechanisms between nanoparticle-polymer and macroscopic mechanical response of polymer nanocomposites (*32, 33*). When loading of NPs in polymer matrix remains low, commonly very modest enhancement of PNC's modulus is observed bellow T_g which is consistent with micromechanics models. However, vast enhancement of PNC's modulus is observed around and above the glass transition (Figure 2 A). In the field of PNCs, two reinforcing mechanisms are respected among the researchers: *i*) altered relaxations of polymer by its immobilization in the presence of inclusion (*34-42*) and *ii*) sort of stress-transfer via interconnected particle superstructures (*41-52*).

The mechanical properties of magnetically assembled nanoparticle system was studied by various authors using different matrix systems filled with micro (*20*), sub-micro (*19*) or nano sized magnetic particles (*13, 15, 53, 54*). These experiments exhibit increased modulus of the composites with longitudinally oriented particle structures. While strong anisotropy is observed when longitudinally, transversely and/or randomly oriented and structures samples are compared (Figure 2 B,C). Mechanical properties were usually investigated in close proximity

or far above of T_g of the polymer matrix. However, mechanisms for the reinforcing effectivity of anisotropic structures rather left unanswered.

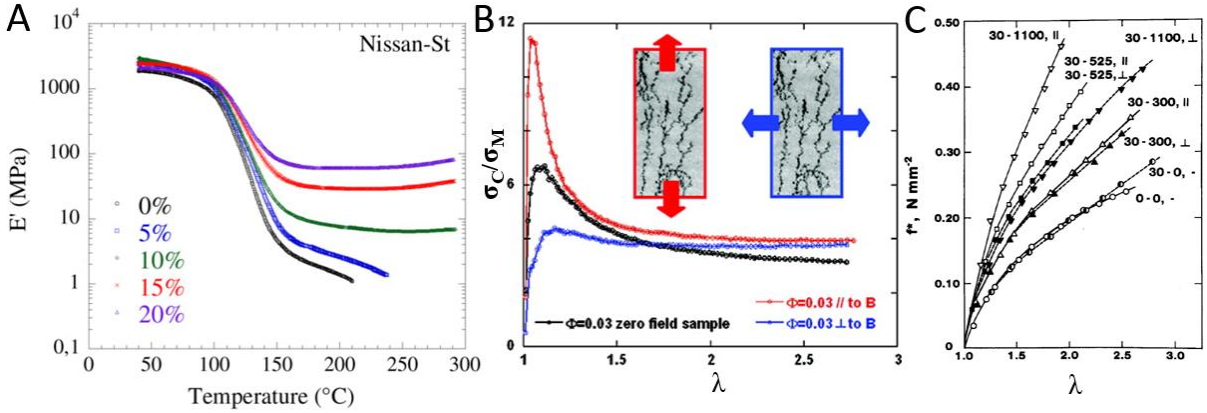

Figure 2 (A) DMA temperature ramp of self-assembled PS/SiO_2 PNCs with an increasing volume fraction of SiO_2 indicated by the legend in the graph. Reprinted from ref. (*42*), Copyright (2012), with permission from Elsevier. (B) Normalised reinforcing effectivity of magnetically assembled PS/γ-Fe_2O_3 nanocomposites to the neat PS matrix as function of draw ratio (λ) with depicted structures and measured directions. Reprinted with permission from ref. (*15*). Copyright 2011 American Chemical Society. (C) Stress-strain curves for PDMS matrix (○) and its composites containing 30 wt. % of sub-micro magnetic particles assembled in the absence of magnetic field (◐) and increasing magnetic field (▲) 300, (■) 525 and (▼) 1100 Gauss. Empty and filled symbols are for longitudinal and transverse direction, respectively. Reprinted with permission from ref. (*143*). Copyright 1987 John John Willey and Sons and Sons.

Aim of thesis

Impulse of external magnetic field initiates controlled assembling process of magnetic nanoparticles into ordered nano and microstrucutres. Magnetic dipole interactions are driving force of this process and dependent on the strength of external magnetic field, while environmental resistance of polymer matrix counteracts against these forces. Also, initial particle packing has a large impact on the balance of magnetic forces between particles and determines the size and structure of primary assembling blocks. The aim is to evaluate the influence of these processing parameters on the resulted structure with a respect to the kinetics of this process. Structural parameters will be used for interpretation of mechanical properties of these nanocomposites.

2 Materials and methods

2.1 Sample preparation

Photocurable resin was composed from two methacrylate monomers. The first one is poly(ethylene glycol) dimethacrylate (PEGDMA) (99 %, Sigma-Aldrich, USA), with a molecular weight of PEG part, $M_{n(PEG)}$=750 g·mol^{-1} and total molecular weight of monomer molecule is M_r=904.0 g·mol^{-1}. Ethoxylated bisphenol A dimethacrylate monomer (bis-EMA) (>87%, Esschem Europe, United Kingdom) with a molecular weight M_r=496.6 g·mol^{-1} was used as a second monomer. Monomers were mixed in the molar ratio 22/78 and 1 molar % (0.75 wt. %) of phenylbis(2,4,6-trimethylbenzoyl)phosphine oxide (BAPO) (97%, Sigma-Aldrich, USA) was added into the mixture of the monomers as a photo initiator absorbing the light on the edge of blue and UV range with a strong absorption at 371 and 400 nm (*55*). The photocurable resin mixture was used as the master batch for the preparation of PNCs.

The synthesized magnetite nanoparticles were used as a magnetic filler in photocurable polymers and colloids. Particle exhibits spherical morphology and log-normal distribution of diameters with mean diameter, d=16 nm. The weight of particles corresponding to 1 or 2 vol. % was added into 40 ml of the photopolymer resin and subjected to continuous ultrasound dispersion for 1 hour with ultrasound homogenizer Sonoplus HD 3200 (Bandelin, Germany) while rapid cooling of suspension. Residual acetone was removed by the vacuum rotary evaporation at laboratory temperature while reaction mixture was shielded against the light to avoid the photopolymerization in thin layers on the walls of the flask. After the removal of acetone, the particle suspension in photopolymer was subjected to second step of continuous ultrasound dispergation for 5 hours with ultrasound homogenizer Sonoplus HD 3200 (Bandelin, Germany) while rapid cooling of suspension.

Small volume of the particle suspension was drop casted between two quartz glass microscopy slides covered with a thin cellophane foil. The mould was placed on quartz glass platform in the center of the solenoid. Magnetic field (B=0, 5, 25, 50 mT) was applied for entire time of the sample preparation. After certain time of magnetic irradiation (t_a=0, 5, 10, 20, 30, 60, 300 sec) for the particle assembly, UV light generated by the light source OmniCure S2000 (Excelitas Technologies, USA) was applied for 5 minutes for each side of the sample. Walls of the solenoid were covered with an aluminium foil for the light. Intensity of emitted light was measured as 40 mW·cm^{-2} in the sample preparation area. After photopolymerization, thin film samples were demoulded and post cured in a vacuum oven at 100 °C for 1 hour under vacuum.

2.2 Structural analysis

The morphology and size of particles, structure of the nanocomposites and particle assemblies was investigated by the scanning electron microscope (SEM) Mira3 XM (TESCAN, Czech Republic) in secondary electrons (SE), back-scattered electrons (BSE) and/or in transmission mode (STEM). Also, high-resolution transmission electron microscope (HR-TEM) TITAN Themis (FEI, USA) was used. Samples for SEM were polished using TEM Mill 1050 (Fischione Instruments, USA) and very thin layer of the sample surface was milled off for the structures to be observable by the electron microscopy. Thin slices for STEM and HR-TEM were prepared by Ultramictome EM UC7 (Leica Microsystems, Germany). Nanoparticles were drop casted from the diluted acetone suspension onto the carbon film coated TEM grid or deposited on the SEM sample holder.

2.3 Dynamic mechanical analysis

Dynamic mechanical analyzer for the solid samples RSA G2 (TA Instruments, USA) was used for the measurements of thermo-mechanical properties of the samples in tension with an axial

deformation of ε=0.05 %, frequency f=1 Hz and top-down temperature ramp from 170 °C to -100 °C with a cooling rate 5 °C/min. Cooling from 170 °C was used to erase thermal history of the sample. Geometry of thin film photocured samples was as follows: loading gap l=10 mm, width w=6 mm and film thickness t=80 μm. At least two samples were used for the measurements and their mean value with a standard deviation is presented.

2.4 Magnetic properties

Magnetic properties of synthesized magnetic nanoparticles were measured with a use of Mini Cryogen-Free Magnet System (Cryogenic Limited, United Kingdom) at the laboratory temperature T=298 K (temperature of assembling). Magnetic properties exhibit a ferrimagnetic behavior with a hysteresis of magnetization and remanence.

3 Results and discussion

3.1 Structure

3.1.1 Self-assembly aggregation, B=0 mT

Initial self-assembled structures exhibit relatively extensive aggregation of MNPs into sub-micron irregularly shaped assemblies with small aggregates (quasi isotropic, composed from few particles) homogenously distributed in the sample volume (Figure 3). Lower particle loading, 1 vol. %, exhibits rather isolated particle aggregates (Figure 3A) in contrary to 2 vol. % sample with considerably bigger and microscopically percolated particle structures (Figure 3B). The adsorption of low molecular weight photopolymer monomers such as those used in the experiments apparently cannot sufficiently stabilize the particle dispersion by the steric repulsion despite the presence of numerous polar bonds in PEG chains and ester bonds (~**CO–O**–CH_2–CH_2–**O**~). It will be later shown that close MNPs are spaced with a thin layer of polymer and structures are something between aggregate and cluster. Despite various stabilizing strategies, problematic dispersion and spontaneous aggregation of MNPs in photopolymer matrix (*31, 56, 57*), other polymer solutions and melts (*14, 58-63*) has been reported also previously by numerous researchers.

It was proposed that aggregation of MNPs in liquid polymer matrix undergoes two steps aggregation process (*13, 60*). In the first step, primary aggregates composed from few of particles (for example 10) are created via interparticle interactions such as van der Waals, or electrostatic (including the magnetic attraction is highly reasonable). In the second step, primary aggregates form the secondary fractal aggregates as a volume fraction of MNPs increases above ϕ>0.01 vol. %. Few isolated, most probably kinetically entrapped, self-assembled structures consisted from several particles with a diameter ~50-100 nm and little bit larger ~150 nm for ϕ=1 and 2 vol. %, respectively were found within the polymer matrix. Small number of even smaller (few particle) aggregates and single particles were found during the analysis of multiple STEM images at high magnifications, but the presence of these objects is rather exceptional and rare. Despite the origin of the primary aggregates (dispersion of powder vs. self-assembly aggregation) is uncertain, these small objects are building blocks for any other structures which further grow in the system with or without the external magnetic field. They either exist in the colloid suspension from the beginning or they are formed very quickly. Fractal-like aggregates in this work such as those in Figure 3 were created by a complex multi-step aggregation of smaller particle structures (primary aggregates) into large fractal aggregates with an irregular. Two populations of primary aggregates of different shape and size were observed. The isotropic spherical and anisotropic aggregates with elliptical shape a slightly larger number of particles and volume.

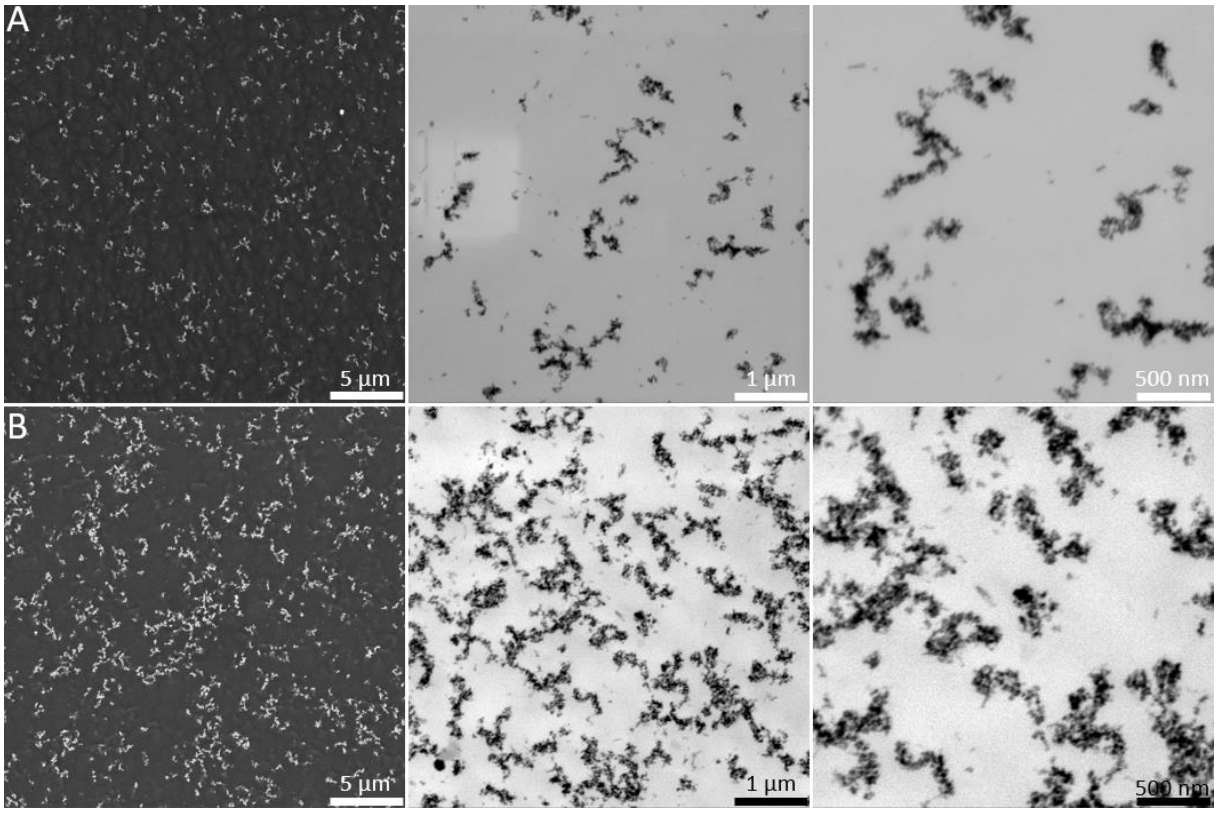

Figure 3 Electron microscopy images of the particle structure in the photopolymer matrix at filler loading (A) ϕ=1 vol. % and (B) ϕ=2 vol. % in absence of the external magnetic field, B=0 mT. BSE and STEM modes, magnification: 10k, 50k and 100k x.

Remanent magnetization measured at the zero field accompanied by the particle aggregation was experimentally observed by Robbes, et al. (*60*) or Bharti, et al. (*64*), however, effect of the magnetic interactions on the aggregation process was not studied. To address the relative strength of van der Waals and magnetic interactions on the aggregation process, corresponding energetic potentials were calculated and normalized to thermal energy (Equation (1)). Mean interparticle surface-to-surface distance (*33*) and mean shortest interparticle surface-to-surface distance (*39*) for randomly packed spheres is used assuming homogeneous initial dispersion of MNPs at filler loading ϕ=1 and 2 vol. %. (see Figure 4A).

Energy of van der Waals attraction between magnetite nanoparticles is calculated according to Equation (2) (*59*).

$$U_{\mathrm{Thermal}} = k_{\mathrm{B}}T \qquad \text{Equation (1)}$$

$$U_{\mathrm{vdW}} = -\frac{A}{12}\left[\frac{d^2}{l^2-d^2} + \frac{d^2}{l^2} + 2ln\left(1-\frac{d^2}{l^2}\right)\right] \qquad \text{Equation (2)}$$

$$\gamma = \frac{U_{\mathrm{vdW}}}{U_{\mathrm{Thermal}}} = \underbrace{\left|-\frac{A}{12}\left[\frac{d^2}{l^2-d^2} + \frac{d^2}{l^2} + 2ln\left(1-\frac{d^2}{l^2}\right)\right]\right|}_{\text{van der Waals Energy}} \Big/ \underbrace{k_{\mathrm{B}}T}_{\text{Thermal Energy}} \qquad \text{Equation (3)}$$

Where A is Hamaker constant ($A_{Fe_3O_4}$ =2.1·10^{-19} J (*59*)), d is the particle diameter and l is the center-to-center interparticle distance. Boltzmann constant k_B=1.38·10^{-23} J·K^{-1}, temperature of assembling process T=298.15 K.

Magnetic energy between two particles with a parallel moment orientation (θ=0 °) was calculated according to Equation (4) (*64-67*).

$$U_{\text{Mag.}} = \frac{\mu_0 M^2 (1-3\cos^2\theta)}{4\pi l^3} \qquad \text{Equation (4)}$$

$$\lambda = \frac{U_{\text{Magnetic}}}{U_{\text{Thermal}}} = \underbrace{\left|\frac{\mu_0 M^2 (1-3\cos^2\theta)}{4\pi l^3}\right|}_{\text{Magnetic Energy}} \Big/ \underbrace{k_B T}_{\text{Thermal Energy}} \qquad \text{Equation (5)}$$

Where μ_0 is the magnetic permeability of free space $\mu_0 = 4\pi \cdot 10^{-7}$ H·m^{-1}, magnetic moment bear by a single particle $M = 9.74 \cdot 10^{-19}$ A·m^2 and θ is the angle between magnetic moment and center-to-center interparticle distance ($\theta = 0°$).

Both energies were normalized to thermal energy (Equations (3) and (5)) and their normalized values in the units of thermal energy are plotted as a function of interparticle surface-to-surface distance in Figure 4B.

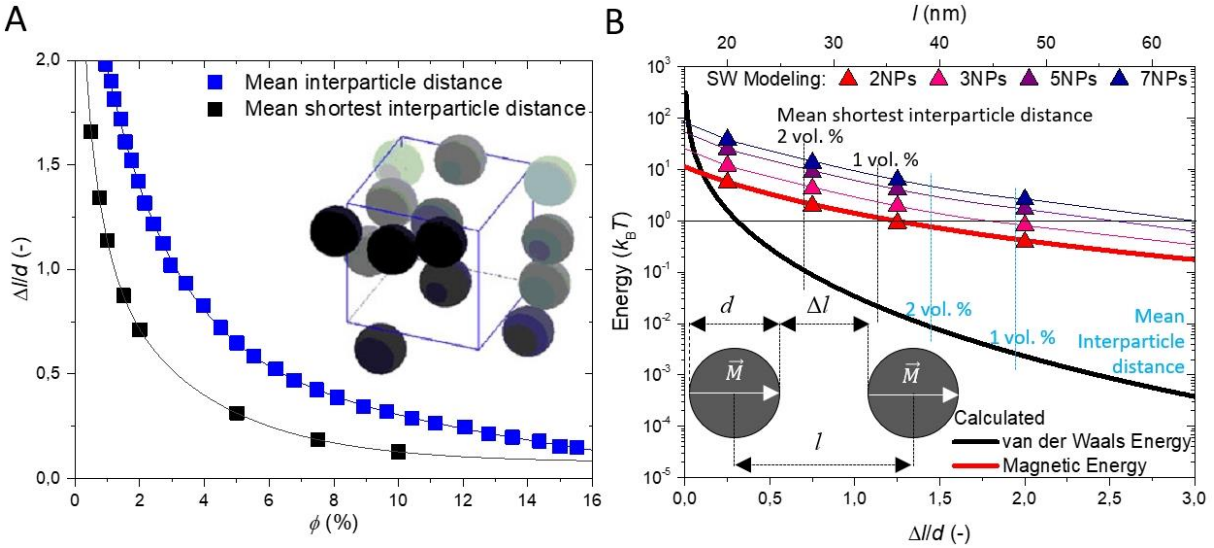

Figure 4 (A) Mean interparticle distance normalized to the particle diameter as a function of filler volume fraction, data acquired from ref. (*33*, *39*). Inset shows structure of PNC with a random particle packing. Reprinted from ref. (*33*), Copyright 2010, with permission from Elsevier. (B) Calculated van der Waals (solid black line) and magnetic interaction energy (solid red line) between two MNPs, d=16 nm as a function of their interparticle distance in the units of thermal energy ($k_B T$). Inset depicts the particle arrangement. Triangles represent micromagnetic simulations of mutual magnetic interaction energy for increasing number of in-line aligned MNPs: 2–red, 3–pink, 5–purple and 7 MNPs – blue.

Energy of van der Waals attraction scales with an interparticle distance and it significantly contributes to aggregation only at very short interparticle distances. vdW energy dramatically overcomes the effect of long-range magnetic attraction bellow Δl<1.75 nm. Even shorter interparticle distances can be found in the particle aggregates and vdW interactions can be strong stabilizing forces holding the aggregates together. On the other hand, van der Waals interactions become too weak above Δl>5 nm to overcome the thermal motion of the particles and these forces are not strong enough to bring the remote MNPs to close contact.

Magnetic interactions contribute to aggregation significantly on much longer ranges when compared to van der Waals attraction and contributes to aggregation process of two 16 nm magnetite particles up to interparticle distance Δl=20 nm at which λ=1. Magnetic energy for mean shortest interparticle distances satisfactorily falls to the aggregation region (λ>1) while energetic values for mean interparticle distance remain still in diffusion region (λ<1). Interparticle distances exhibit much broader distribution of interparticle distances and

consequently also much shorter distances than reported mean values exist in the system (*68, 69*). After all, this can be seen also in depiction of the model PNC system containing randomly packed spheres in inset of Figure 4A.

3.1.2 Magnetically assembled structures

The application of magnetic field triggered rapid assembling of magnetic building blocks into anisotropic chain-like assemblies with a homogeneous orientation controlled by the external magnetic field. In the magnetic field, particles rapidly form various types of structures and their mutual interactions are enhanced as magnetic moments are more aligned in direction of the field when compared to zero field sample. Magnetic building blocks create stronger local magnetic field resulting from the contribution of external field and magnetization of particles aggregates. Higher extent of alignment, longer and larger structures are assembled under higher external magnetic fields as can be seen in Figure 6. The anisotropic structures are perfectly oriented in the field direction. One-dimensional structures are gradually merged in longitudinal and lateral direction and create superstructures under intense external fields, higher particle loading or extended assembling times.

The images of electron micrographs were analysed in ImageJ software to obtain the volume of the structures, their length and diameter (width) resulting in the aspect ratio. These structural parameters for analysed structures are reported in Figure 5.

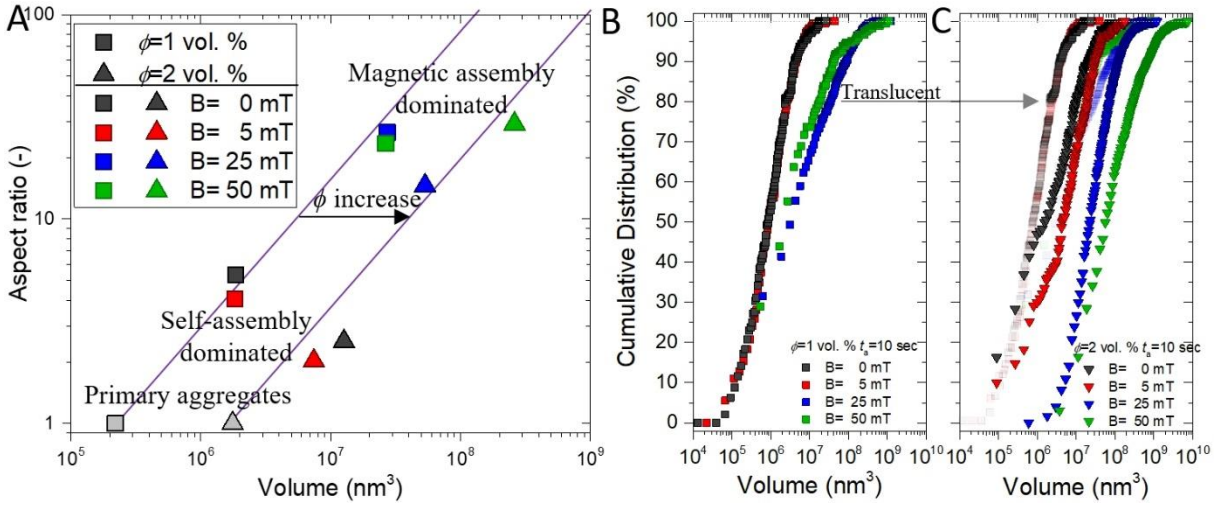

Figure 5 (A) Mean volume versus mean aspect ratio for the structures assembled after t_a=10 sec. Cumulative distribution of structure volume (B) for ϕ=1 vol. % and (C) for ϕ=2 vol. % assembled after t_a=10 sec. In (C) translucent data represent ϕ=1 vol. % for the comparison.

3.1.2.1 Assembling in low magnetic field, *B*=5 mT

At a low particle concentration, ϕ=1 vol. %, magnetic structures are elongated along the field direction and assembled into superstructures guided by the low magnetic field, *B*=5 mT. These superstructures are formed from the individual aggregates interconnected by head to tail magnetic interactions acting between them (Figure 6). These superstructures are homogenously oriented along the field direction. Two processes proceed simultaneously in this system with a low magnetic field: *i*) self-assembly aggregation of MNPs and *ii*) their magnetic alignment. Low external magnetic field, *B*=5 mT, rather results in the concentration, straightening and chaining of adjacent (self-assembled) neighbouring aggregates into large superstructures along the imaginary force lines of the magnetic field while self-assembly process has a major effect on the growth of individual aggregates. Increased loading of MNPs, ϕ=2 vol. %, shows transition from the anisotropic sub-micro aggregates to microscopically percolated assemblies (Figure 6) with no preferential alignment or anisotropy which is further developed after the

extended assembling times. These microscopic flocculates are created by the drag and concentration of the magnetic material in one spot and thus large particle-free domains are formed.

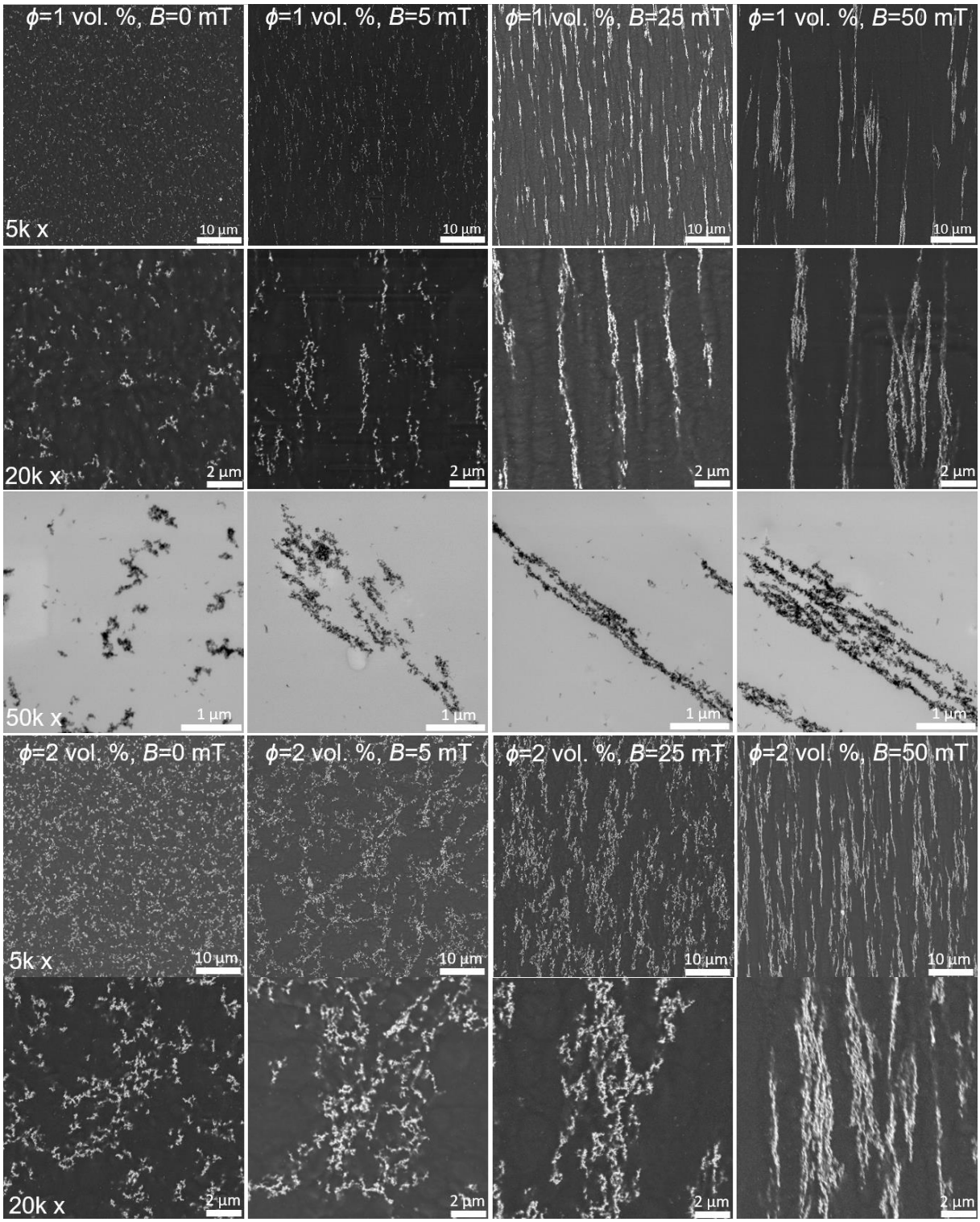

Figure 6 SEM and STEM images of self-assembled structure in absence of external magnetic field and magnetically directed self-assembled structures in presence of external magnetic fields B=5, 25 and 50 mT at particle loading ϕ=1 and 2 vol. %, after t_a=10 sec. Images at increasing magnification: 5k, 20k× in BSE and 50k× in STEM mode.

3.1.2.2 Assembling in higher magnetic fields, *B*=25 mT and *B*=50 mT

Increase of magnetic field to *B*=25 mT and 50 mT led to more rapid organization of MNPs into well-developed anisotropic structures with a high aspect ratio (in the system containing ϕ=1 vol. %). Magnetic material is concentrated along the imaginary force lines of the field. Again, structures are homogenously oriented with a long axis of the magnetic chain backbone aligned along the direction of the applied magnetic field. From both SEM and STEM images (Figure 6), it is clearly seen that these superstructures are built from individual particle chains that are several particles wide and micrometres long. These one-dimensional structures interact with each other by head-to-tail magnetic interactions creating longitudinally interconnected superstructures. The widening of the structures is caused by an instability of repulsive interchain magnetic interactions which results in their lateral merging and formation of chain junctions. This is especially visible for the strongest magnetic field, *B*=50 mT. Large magnetic structures are surrounded by stronger magnetic field while smaller assemblies have a higher mobility in viscous matrix. Growing structures gradually attract and absorb smaller magnetic building blocks from 3D area around them during the magnetic directed self-assembly and increase their volume (*22*, *64*).

The diameter of the magnetic chains is very close to diameter of primary aggregates found in nanocomposites. With a diameter ~100 nm, aspect ratio (*L*/*D*) of the structures easily exceeds the values ~100. However, mean values of chain's aspect ratio lie around ~25-29 due to presence of shorter structures (see Figure 6 for *B*=25 and 50 mT in low magnification). This is more evident and frequent for the structure assembled under *B*=50 mT. The length of some particles assemblies considerably exceeds the length of those assembled under *B*=25 mT but lot of relatively short and thick particle chains are found in the system as well, which consequently decrease mean length/aspect ratio when compared to system assembled under *B*=25 mT. As well, these structures show larger extent of lateral merging but they still remain mainly individual with a spacing polymer between them. Additional lateral merging of the structures is more obvious after extended assembling time or increased concentrations of MNPs (discussed further in text). The assembling of the individual particle chains into one dimensional particle superstructures is a perfect example of complex bottom-up built-up approach.

3.1.2.3 Kinetics of assembling and growth of superstructures

For the low magnetic field *B*=5 mT and low particle loading ϕ= 1 vol. %, very slow process of structure growth is visible, especially at images of lower magnifications (Figure 7). Structures rather grow in direction of magnetic field and lateral merging starts to occur after longer assembling times (such as t_a>30 sec.) and with obvious lateral merging after very long assembling times, t_a=300 sec. The structure rapidly changes in the system with ϕ= 2 vol. %. Here, the switching of the low magnetic field attracted building blocks and increased their concentration in specific points promoting phase separation. This creates particle-free and particle-rich domains. On the other hand, the volume of magnetic objects does not dramatically differ from the self-assembled structure (Figure 5). With an increase of assembling time, situation changes and concentrated aggregates grow, elongate in the field direction and they are densified. Sort of particle micro web very similar to macroscopically percolated fractal-like aggregates is generated in the matrix. After prolonged assembling time, t_a=300 sec., drastic reconfiguration of the particle structure is observed. Particles are organized in microscopic chain-like structures with a homogeneous orientation while lateral branching diminish. This transition from the branched and percolated structure occurs somewhere in the range t_a=60-300 sec. This structure would slowly grow further to one-dimensional macro structure.

Faster growth of the superstructures is observed for assembling in higher magnetic fields with substantial development of micro superstructures and coarsening of system within short time

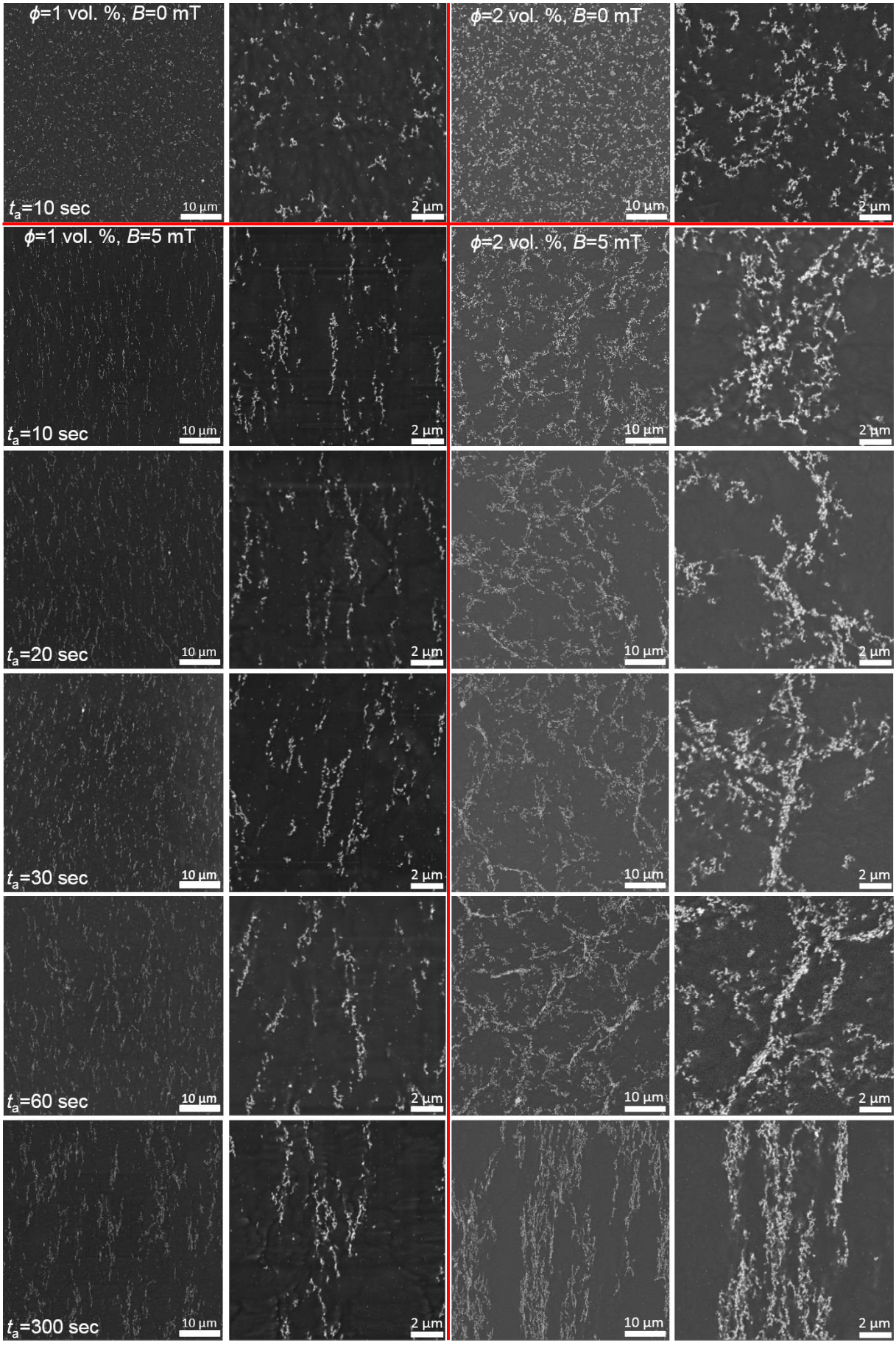

Figure 7 Electron micrographs of magnetically directed self-assembled structures in the photopolymer matrix containing 1 and 2 vol. % of Fe_3O_4 nanoparticles at the magnetic induction B=0 mT and B=5 mT after t_a=10, 20, 30, 60 and 300 seconds. Magnification 5k and 20k x in BSE mode is provided for each sample.

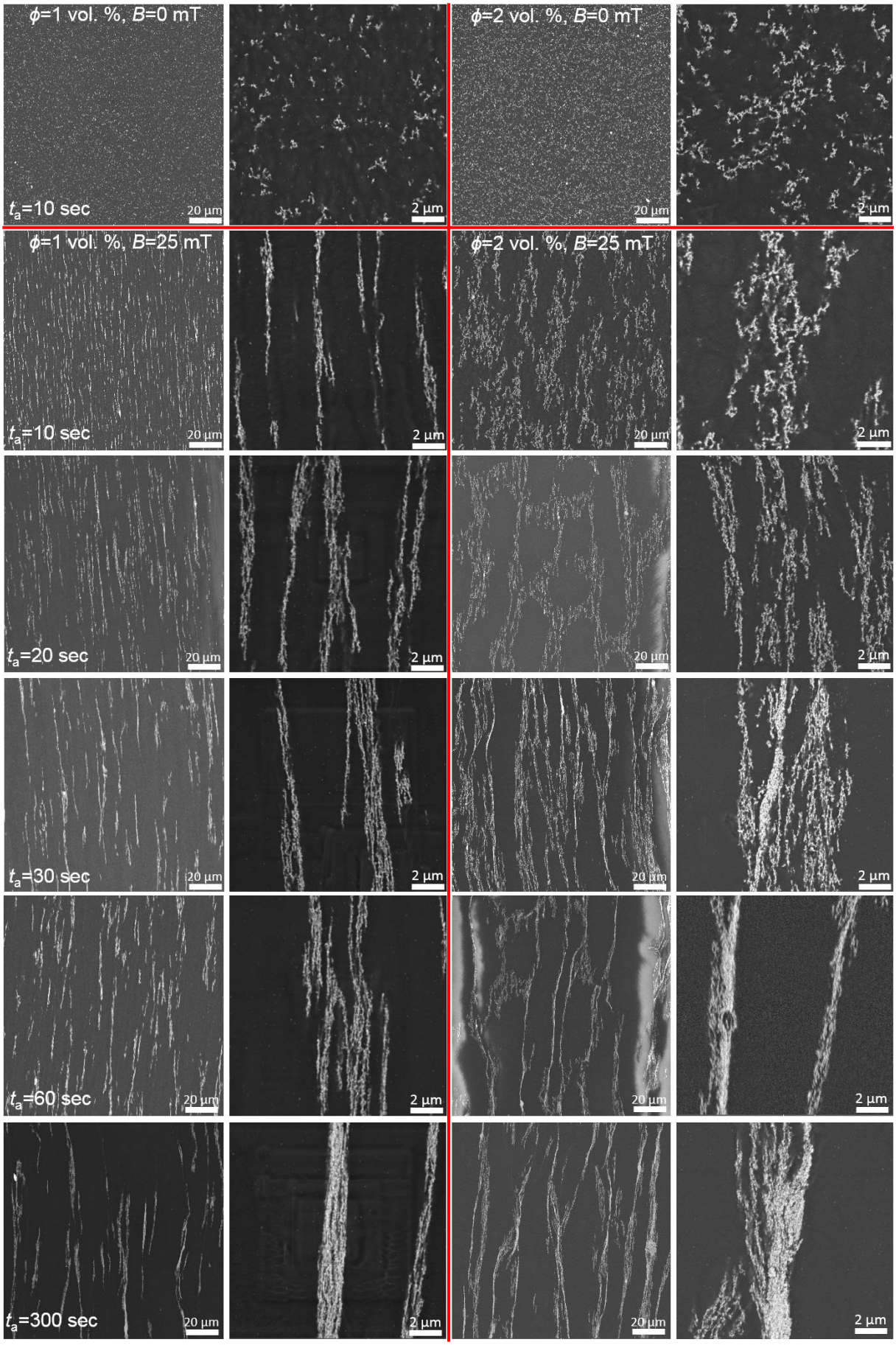

Figure 8 Electron micrographs of magnetically directed self-assembled structures in the photopolymer matrix containing 1 and 2 vol. % of Fe_3O_4 nanoparticles at the magnetic induction B=0 mT and B=25 mT after t_a=10, 20, 30, 60 and 300 seconds. Magnification 2k and 20k x in BSE mode is provided for each sample.

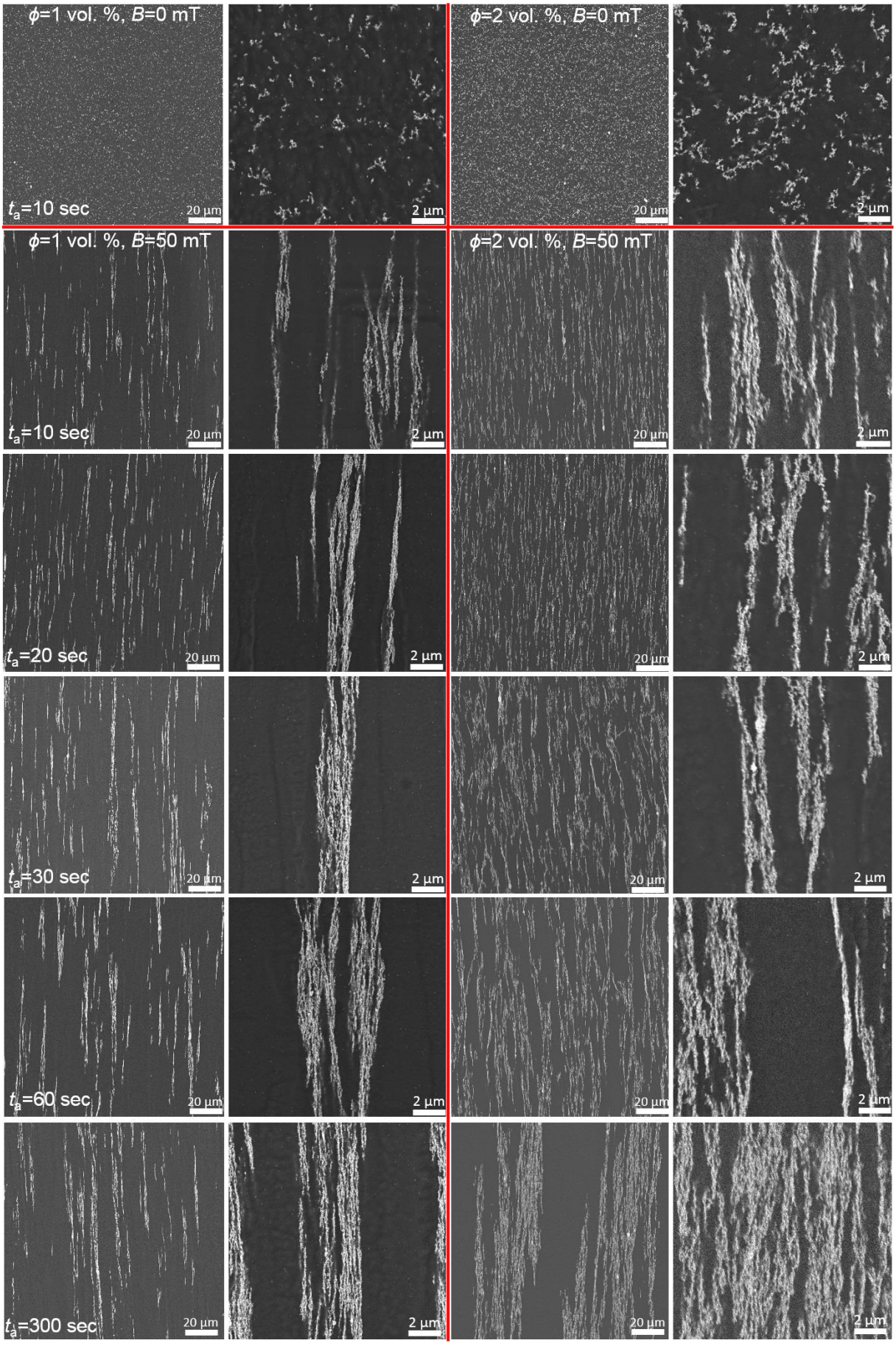

Figure 9 Electron micrographs of magnetically directed self-assembled structures in the photopolymer matrix containing 1 and 2 vol. % of Fe_3O_4 nanoparticles at the magnetic induction B=0 mT and B=50 mT after t_a=10, 20, 30, 60 and 300 seconds. Magnification 5k and 20k x in BSE mode is provided for each sample.

scales. The growth of the structures is clearly visible in Figure 8 and Figure 9 for B=25 and 50 mT, respectively. The transition from nano-/submicro- to micro- and macrostructure occurs within very short assembling times (t_a>30 sec.). Magnetic field B=25 mT forms micro chains in both particle concentrations (1 and 2 vol. %) after t_a=300 seconds, and these particle chains are stable. They also display a relatively large densification. In magnetic field B=50 mT, extremely large magnetite-rich micro islands are created via significant lateral merging after 300 seconds of assembling. Interaction of magnetic chains in lateral direction is significant for magnetic field 50 mT.

3.2 Thermo-mechanical properties

The mechanical anisotropy of magnetically assembled nanoparticle systems was studied by various authors (*13, 15, 19, 20, 53, 70-73*). Despite research done in this field, reinforcing mechanisms of anisotropic chain-like particle structures are not fully understood yet.

3.2.1 Glass transition

Glass transition of neat polymer matrix (PEGMA/bis-EMA=22/78) was evaluated as T_g=45.1±3.9 °C. Its position shifts to lower temperatures and decreases by more than ΔT_g>-5 °C with an addition of 1 vol. % of magnetic nanoparticles which are aggregated into complex sub-micro structures (Figure 10B). This decrease is caused by the absorption of the light during the photocuring by magnetite nanoparticles and especially by their larger aggregates/structures (*31, 56*). Particle structures work as efficient light absorbers/scattering objects for the light despite their diameter is bellow critical dimension which equals to wave length absorbed by the photoinitiator (λ=370-400 nm)(*55*). For larger structures than this length, penetration of light is almost impossible. Light required for initiation and cleavage of photoinitiator thus may not penetrate properly the depth of the sample which is even pronounced for growing structures in magnetic field. With an increase of interchain distance occurring at B=25 and 50 mT, light penetrates trough the magnetite free domains – optical paths of neat matrix and T_g starts to upturn (*31*). In addition, light has limited possibility to penetrate inner structure of particle assemblies and cross-link the monomers entrapped here. Later, it will be shown that this polymer fraction is essential for thermo-mechanical properties of PNCs. Thermal post curing generates additional initiating radicals and repeatably trigger the cross-linking radical polymerization, however mobility of free radicals is slower and limited by the diffusivity of free radicals trough the polymer network although temperature is far above T_g.

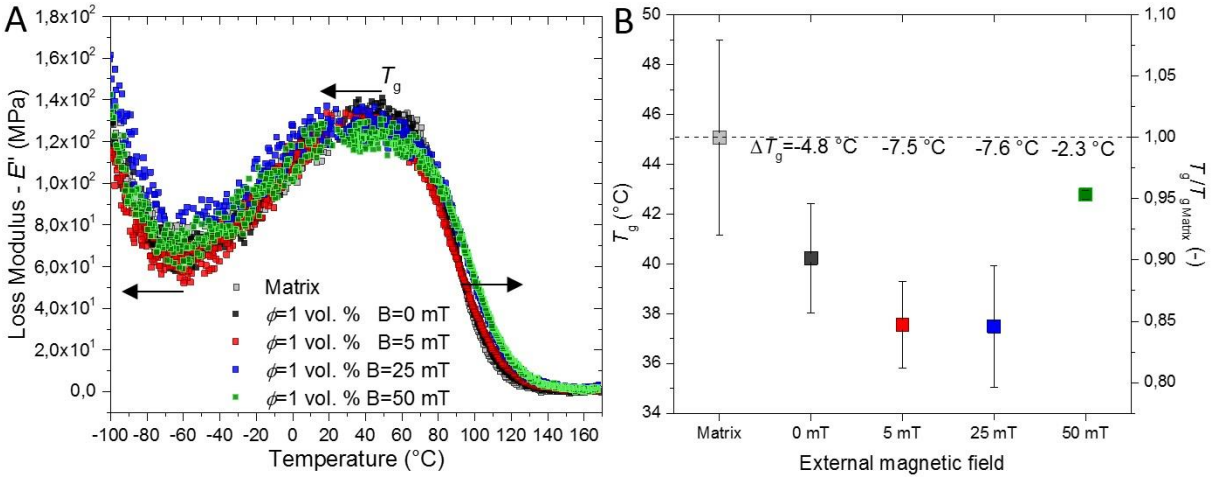

Figure 10 (A) Loss modulus for the matrix and nanocomposites containing ϕ=1 vol. % of self- and magnetically-assembled Fe_3O_4 magnetic nanoparticles. (B) Evaluated T_g of the polymer matrix and its nanocomposites as a function of the external magnetic field.

The presence of the immobilised layer of polymer on the NPs is assessed by various analytical methods (*74*) but the most commonly, the increase of T_g of composite is the most straight forward evidence of altered relaxations. Due to decrease of cross-linking density with an addition of MNPs and their structuring by magnetic interactions, T_g of PNCs is gradually decreasing (*75*), hence the presence of polymer chains with retarded dynamics cannot be qualitatively and directly evidenced by analysis of T_g. On the other hand, this does not mean that polymer chains are not immobilised/confined by particle surface. The polymer network in the presence of MNPs just has a smaller cross-linking density than the unfilled matrix. Repulsive NP-polymer interaction is not expected.

3.2.2 Mechanical properties in glassy region

The complete temperatures spectrum (from -100 °C to 170 °C) of the storage moduli of the magnetic PNCs is shown in Figure 11A,B for both longitudinal and transverse direction, respectively. Insignificant effect of the particles and their assemblies on the mechanical response is observed bellow glass transition of the system while substantial difference in modulus is observed above glass transition. Storage modulus is normalized to modulus of neat polymer matrix for both regions – glassy and rubbery and shown in graph in Figure 11C.

Mechanical properties of composites in glassy region scatter around boundary E/E_M=1 regardless of structure size or its orientation (Figure 11C). Negligible effect of NPs on the stiffness of PNCs in the glassy region is commonly known for decades. In this region, mechanical response of PNCs obeys a micro-mechanical reinforcement given by the volume replacement mechanism – replacement of polymer with a stiffer phase (particles). This model accounts with a contribution of particle deformation to overall macroscopic deformation of PNC. And thus, it might be said that addition of fraction of 1 vol. % will have only marginal effect on the mechanical robustness of PNCs. Usually, higher volume fractions (or substantial modification of polymer matrix via particle-polymer interactions) are required to induce reinforcement of the glassy matrix. Experimental data of the storage modulus were fitted with a micro-mechanical Kerner-Nielsen-Lewis model which is commonly utilized for the particle filled polymers filled either with MPs or NPs (*76*). This model predicts a stiffness of PNCs filled with ϕ=1 vol. % of MNPs as E_{KNL}=3.5 GPa which corresponds to normalized value E_{KNL}/E_M=1.021 (Figure 11C – blue dotted line). Data of glassy state modulus scatter around this trend line what means that reinforcing mechanisms can be explained by the volume replacement of softer polymer glass with much stiffer magnetic nanoparticles.

3.2.3 Mechanical properties in rubbery region

Rubbery modulus of neat matrix drops down by two orders of magnitude from glassy state with a stiffness E_M^G=3.43GPa to E_M^0=68.6 in rubbery plateau. In contrary to glassy region, large enhancement of composite stiffness and strong anisotropy was measured for the mechanical properties of PNCs far above their T_g. Relative values of the composite stiffness normalized to neat polymer modulus are plotted in Figure 11C. Difference between mechanical properties of polymer matrix and its PNCs starts to appear in proximity of the T_g of the polymer matrix. Course of storage modulus as well of tan δ starts to separate around T=20 °C and their different course becomes significant with an increasing temperature as soon as T_g is exceeded. For transversely oriented structures, almost constant enhancement of the rubbery modulus was measured comparable with a modulus of the self-assembled composites (Figure 11B,C). As well, tan δ shows same position and height of tan δ peak. Much stronger effect of the particles structures on the increase of the rubbery modulus is observed for their longitudinal orientation (Figure 11A,C) and modulus increases steadily with an increasing assembling field (with a growth of the particle structures in the sample).

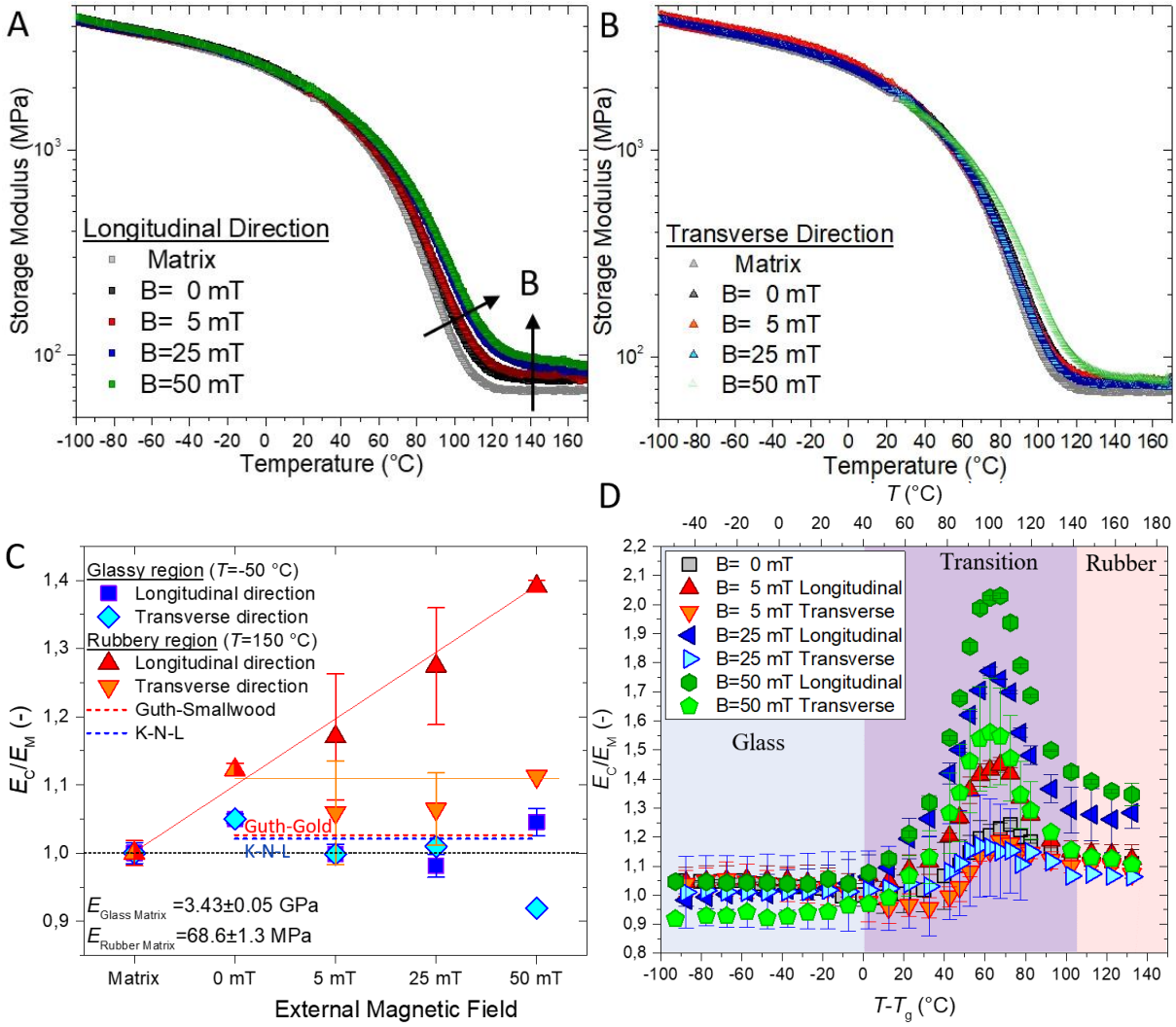

Figure 11 DMA temperature ramp spectrum for photopolymer matrix and its nanocomposites filled with ϕ=1 vol. % of Fe_3O_4 and assembled under magnetic fields B=0, 5, 25, 50 mT after t_a=10 sec. Storage modulus of PNCs films in (A) longitudinal and (B) transverse direction with a respect to the structure orientation as a function of temperature. (C) Storage modulus of composites normalized to modulus of neat matrix (E_C/E_M) as a function of the external magnetic field. (D) Relative composite modulus (E_C/E_M) for PNCs containing ϕ=1 vol. % of MNPS as a function of distance from T_g (T-T_g). Individual temperature relaxation time regions are marked as follows: glass – blue, transition – purple and rubber – red.

Guth-Gold model (*38*, *77-79*) is used for description on the mechanical properties of PNCs above T_g. This model is derived from Einstein's viscosity formula for filled liquids and it is based on the inability of particles undergo the deformation process of their atomistic structure due to large mismatch of matrix/particle moduli and only surrounding matrix is being strained (locally overstained). In the photopolymer system, this model predicts a normalized rubbery modulus of nanocomposite as E^0_{GG}/E^0_M=1.026 (Figure 11C – red dotted line). Experimental data for both, longitudinal and transverse orientation in rubbery state show considerably higher values than a model prediction. Discrepancies between model and real experimental results are the most commonly debated on the background of the immobilized layer (*38*) or contribution form particle structure (*79*) concepts. The both theories seem to have their own logic and their mutual existence might be also explanation despite hardy to distinguish their individual contributions.

Glass transition was found to be in linear dependence with υ_c (*80*). Thus, pure matrix which has the highest value of glass transition, logically, should have largest modulus of rubbery plateau. In other words, if υ_c of polymer matrix decreases, rubbery modulus of polymer matrix in nanocomposite needs to decrease as well and stiffness of the PNCs is expected to follow the trend of their glass transitions. But relative rubbery modulus of PNCs is steadily increasing with a magnetic field applied for the assembling beyond the limit set by Guth-Gold model despite T_g decrease (Figure 11C). Two processes with an adverse influence on the PNC's stiffness are present: *i*) decrease of the photopolymerization yield and *ii*) stiffening by the particle structures. The decreasing polymerization yield in the presence of NPs and enhancement of composite's stiffness was observed for example by Sotta, et al. (*79*). Normalization of relative value of composite stiffness (E_C/E_M) by the parameter linearly proportional to the cross-linking density was used. Similar approach of modulus normalization is adopted here, and $T_{g\,PNC}/T_{g\,Matrix}$ ratio is used for the normalization of the relative rubbery modulus (Equation (16)). This will consequently decrease the value of matrix's modulus, E_M in composite systems.

3.2.4 Mechanical properties in transition region

Relative values of PNC's modulus were plotted as a function of distance from the PNC's T_g (Figure 11D) to address the influence of the particle assemblies on the stiffness of PNCs in whole temperature range – glassy, transition and rubbery region. The effects in glassy and rubbery regions were already discussed in previous sections. Note that T_g of individual composites (Figure 10) were used for the calculation of temperature distance (T-T_g). Large peak of relative composite stiffness can be observed in transition region exhibiting temperature dependent and viscoelastic reinforcement. Maximum is temperature independent for all samples regardless of structure size of its orientation. Note that self-assembled and magnetically assembled structures (B=0, 5, 25 mT) with a transverse orientation shows almost identical course of reinforcing effectivity.

3.2.5 Reinforcing mechanism

The modification of PNCs mechanical response is often attributed to adsorption of polymer chains on the surface of solid inclusions leading to creation of bound layer with altered relaxations (*81, 82*). The thickness of bound layer is usually reported in the order of several nanometres (1-2 nm) depending on various chain properties and interactional strength (*81, 83-86*). For example, Xu, et al. (*87*) studied the adsorption of low molecular weight polypropylene glycol (PPG) on the silica NPs structured in continuous network and its contribution to viscoelastic and thermal response of PNCs. Anderson, Kim and Zukoski (*88, 89*) reported an adsorption of polyethylene glycol (PEG) with various molecular weights on the surface of silica NPs. Both teams reported bound polymer layer with a thickness in order of several nanometres for studied glycol molecules. Also, methacrylate esters are frequently reported to be successfully anchoring moiety in the presence of NPs (*38-40, 42, 90*).

Surface of crystalline MNPs is also covered by hydroxyl groups and thus certain level of similarity can be shared with commonly studied amorphous silica filled PNCs. Both, PEG and ester groups can be found in the backbone of PEGDMA and bis-EMA molecules and polymer chains are expected to interact with a surface of MNPs in analogic attractive manner. Both monomers contain multiple reaction sites. The first one is ester group (*90*) bridging methyl methacrylate with PEG unit and each monomer molecule contains two ester groups at the ends of the molecule backbone. The second interaction site is situated on the oxygen in the backbone of PEG. These groups can act as Lewis acids coordinating their electron density with a hydrogen from surface HO– groups (Lewis base) and create hydrogen bonds. Bis-EMA monomer has a short PEG unit (n_{PEG}=1 and 2), on the other hand, PEGDMA monomer with n_{PEG}=16 can offer

number of interaction sites. In addition, adsorption of initiator/initiating radicals on the surface of particles is not known.

If we will assume the existence of immobilised layer on the MNPs surface as well polymer chains bridging the contact between particles (however, could not be directly assessed by the analysis of the loss modulus and T_g), we will obtain hybrid polymer-Fe_3O_4 structures with a high inorganic content. It needs to be noted that usually higher particle volume fractions are required to increase the fraction of bound polymer relative to that bulk chains in such extent that it is possible to macroscopically distinguish the signal from immobilized chains. Here, we are dealing with a particle loading ϕ=1 vol. % and a complication in the form of decreased photopolymerization yield. Despite this fact, changes induced by particle assemblies on mechanical properties are tremendous. Figure 12A shows an inner particle structure of the magnetic chain in sample B=25 mT from STEM observation. Nanoparticles are spaced with a thin layer of polymer. Interparticle surface-to-surface distance between closest neighbours was measured and trimodal distribution is plotted in Figure 12B. Mostly, particles are in direct contacts or distanced within the sub nanometer range. The radius of particles gives an opportunity for polymer occupation of this space. The second distribution peak is around 4 nm and third one around 14 nm. Both are large enough to accommodate the polymer coils or monomers. Other assembling fields exhibit quite similar particle packing and thus structures are something between aggregate and clusters while this nature depends on actual position within particle chain. Interparticle distances are considerable short in magnetically concentrated assemblies and behaviour of such system can find analogy with highly filled PNCs (*91-93*) or even analogy with a structure of platelets in nacre and/or mineralized collagen fibrils in bone (*94*). Polymerization degree of confined monomer units within the structures is not known. It will be assumed that monomers adsorbed on the particles and polymerized in confined space requires minimum space approximately 2Rg=2.4 nm to fit into the interparticle space without the change in chain conformation due to squeezing ($R_{g\ PEGDMA}$≈1.2 nm, approximated to $PEG_{Mw=1000}$ (*89*), gyration radius of bis-EMA is expected to be lower and more anisotropic).

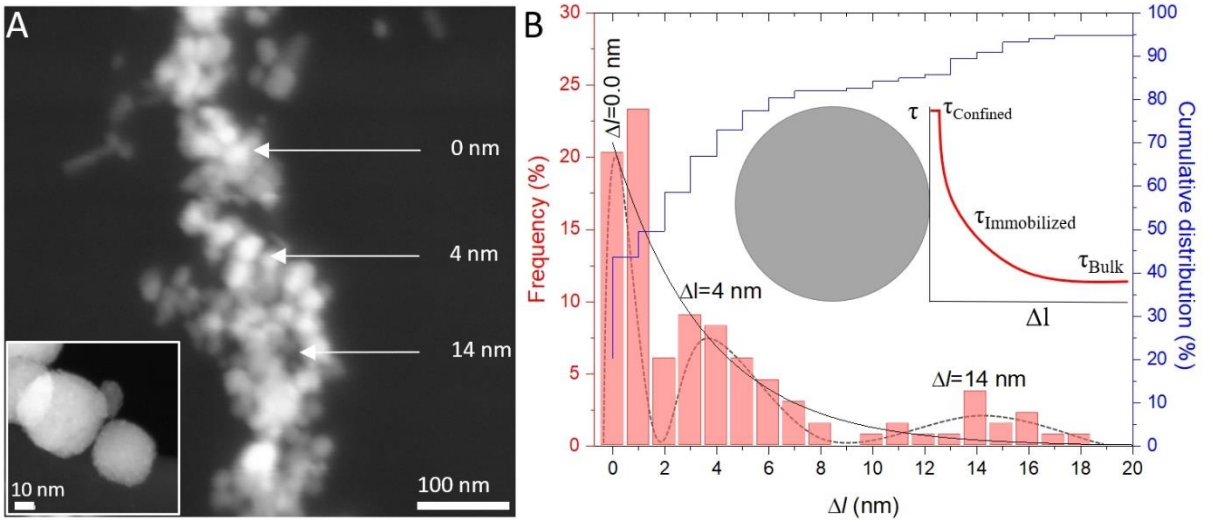

Figure 12 (A) STEM image of anisotropic structure assembled in B=25 mT after 10 seconds with ϕ=1 vol. % of particles in photopolymer matrix (dark areas is polymer). Arrows show typical places with a characteristic spacing. Dark field HR-TEM inset in (A) shows the most frequent situation when particles are in close contact resulting in Δl≈0 nm but their radius gives a rise to non-zero interparticle spacing suitable for polymer bridging. (B) Distribution of interparticle surface-to-surface distances Δl for the closest particle neighbors in the cluster from (A). Inset in (B) shows schematic depiction of relaxation time dependence on distance from particle surface.

In case of the shorter distances ($\Delta l < R_g$), monomer coil cannot occupy this space without further reduction of gyration radius (*93, 95*) or occupation of anisotropic shape (*96*) and consequently drastic modification of chain rigidity.

Various researchers claimed that strongly bound and confined polymer chains may behave as glass even at the temperatures when the bulk polymer is already completely unvitrified. This effect results in the vast increase of reptation/relaxation times, rubbery plateau, or fully disappeared terminal zone commonly evidenced in rheological measurements of highly filled PNCs melts. For example, Mujtaba, et al. (*97*) measured the fraction of surface-immobilized polymer by NMR and detected significant fraction of segments with glassy relaxation times at temperatures of rubbery plateau of SBR/silica PNC. Fraction of glassy segments decreases with a temperature and it is dependent on particle volume fraction and level of confinement (caused by particle percolation). Similar NMR results were also published by Berriot, et a. (*98*) and Chen, et al. (*92*) also outlined that some segments might still appear as glassy in highly filled PNCs melts when interparticle distances are close or even lower than a length of Kuhn's segment. In these systems, unvitrified glass is preserved at particle loadings far above tens of volumetric percent.

Despite very low total fraction of MNPs in our systems, polymers shells are brought close enough to percolate due to magnetic interactions between particles or their assemblies during self- and magnetic assembly. Magnetic field increases local concentration of inorganic content considerably beyond the percolation threshold with a local particle volume fraction inside the particle chains calculated as ϕ_{local}~52 vol. %. This is close to maximum volume occupation for randomly packed spheres. Such short interparticle distances, vast enhancement of rubbery modulus and local particle volume fraction inside the magnetic chains indicate that there might be still a fraction of unvitrified polymer segments trapped inside the particle clusters. Term '*glassy*' will refer to polymer segments with retarded relaxations compared to bulk matrix, in our PNCs.

The percolation of glassy fraction of polymer and creating of continuous glassy backbone in soft matters (above T_g) is believed to be mainly responsible for the thermo-mechanical response of PNCs. Concept of percolated bridging glassy layer seems to be reasonable explanation for thermo-mechanical response of PNCs mainly due to its time-temperature dependence and viscoelastic appearance. Tauban, et al. (*99*) modelled the mechanical response of PNCs with confined polymer chains within the particle structures of various morphologies and packings based on previous experimental results and theories (*98, 100-102*). They present a plot of reinforcing ratio versus distance from T_g which exhibit very similar temperature dependence of reinforcing ratio for highly filled PNCs as plotted in Figure 11D for systems studied in this thesis. Such processing of thermo-mechanical data with a '*bell-like*' temperature dependence and maximum of reinforcing effectivity in transition region is universal for all PNCs. Therefore, distance of PNCs from its *T*g and rubbery plateau is important to be specified in scientific texts dealing with a mechanical response of PNCs! Constant portion of storage modulus of PNCs at temperatures far above T_g is ascribed to deformation of bound glassy polymer with a significantly altered relaxation characteristic and stiffness high enough to avoid modulus drop.

Generally, particles assemblies in PNCs gradually form a nano, sub-micro, mirco and macroscopically percolated hybrid structures of various shapes and geometries with an increasing particle content. Consequently, nano, sub-micro, micro and macroscopic immobilized glassy polymer is formed in soft matrix (*39, 40*) and its shape and geometry are defined by particle arrangement. These hybrid structures can get under the deformation during the sample testing and exhibit non-zero stiffness. In our case, particles are organized in one-dimensional chains – fibers which may carry the load transferred from the matrix. To address

orientation dependent mechanism of reinforcement by hybrid anisotropic structures, continuum micromechanics concepts will be employed. Micromechanics in combination with a model of composite with various structural motives was used to describe the mechanical response of biological hard tissues (*103-105*). Complex reinforcing micro blocks commonly found in biological composites (*94*) were simplified by solid anisotropic microparticles arranged in polymer matrix in special geometrical patterns. Similar concept is used also here despite PNCs shows significant reinforcement only above T_g. Thus, such approximation and adopting of the micromechanical stress-transfer might not be relevant in whole temperature range, for studied PNCs. Hybrid micro chain structures of this work are approximated by solid fibres with a non-zero internal stiffness and homogeneous orientation. Depiction and description of model material with a multi-level hierarchy with images of individual levels of structure is in Figure 13.

During the deformation of the composite, particle fibres are stretched. The stress is transmitted via bridging polymer within the structures and amount of stress carried by anisotropic hybrid structures dependent mainly on their orientation, length and their internal stiffness (E_F). Higher stiffness of hybrid structure than a stiffness of surrounding medium is essential requirement for the composite reinforcement ($E_F > E_M$). In opposite situation, structures will decrease the stiffness of composite. In longitudinal direction, larger portion of stress is transferred from low stiffness matrix while transversely oriented structures are less reinforcing effective (*106*). Hence, transverse direction is comparable with self-assembled quasi-isotropic structures – similar volume of hybrid structures is locally under the deformation.

The internal stiffness of the hybrid structure (E_F) was calculated using semi-empirical Halpin-Tsai model (*106*). This model is commonly used for prediction of the stiffness of polymers filled with micro fibers. Model was set to perfectly fit the experimental data by adjusting the stiffness of fibres (E_F). The stiffness of hybrid fiber in rubbery plateau is around $E_{F\ 150\ °C}$~400 MPa. This value is one order of magnitude higher than stiffness of the surrounding rubbery matrix. Temperature dependency of hybrid fiber structure stiffness is plotted in Figure 14A.

The stiffness of hybrid structure starts to rapidly increase from temperatures somewhere around 130-120 °C which is accompanied by the modulus upturn of its PNC. However, as vitrification of system proceeds the hybrid structure reach the maximum of its stiffness before reaching the T_g of the matrix. Stiffness of the hybrid structure seems to be constant and on the order of glassy matrix modulus far bellow T_g. Thus, it seems that structure was vitrified much earlier and at higher temperatures than surrounding matrix.

Continuum micromechanical interpretation of composite stiffness is only half of the mechanisms relying on load carrying capability of anisotropic structures and their stiffness which originates in nanoscopic interactions. More important question arise: *What causes the mechanical robustness of assemblie*? The finding of bridging laws between continuum macro/micromechanics and nanoscopic interactions might shed a light on the behaviour of complex nanostructures, biological structures and PNCs (*32, 33*). For example, the extent of stress transfer into glass or carbon micro fibers depends on their length projected in tensile direction while their Young's modulus (E_F) is length independent and solely depends on the internal structure and stiffness of chemical bonds. The stiffness of hybrid structures is complex function of all nanoscopic mechanisms which contribute to nanoscopic deformations and hold the particle assemblies together such as: interparticle attractions (van der Waals, electrostatic, magnetic, NP-NP interlocking, friction, etc.), deformation of particle atomistic structure, the strength of NP-polymer interactions and temperature dependent Young's modulus of polymer bridges (*107-109*).

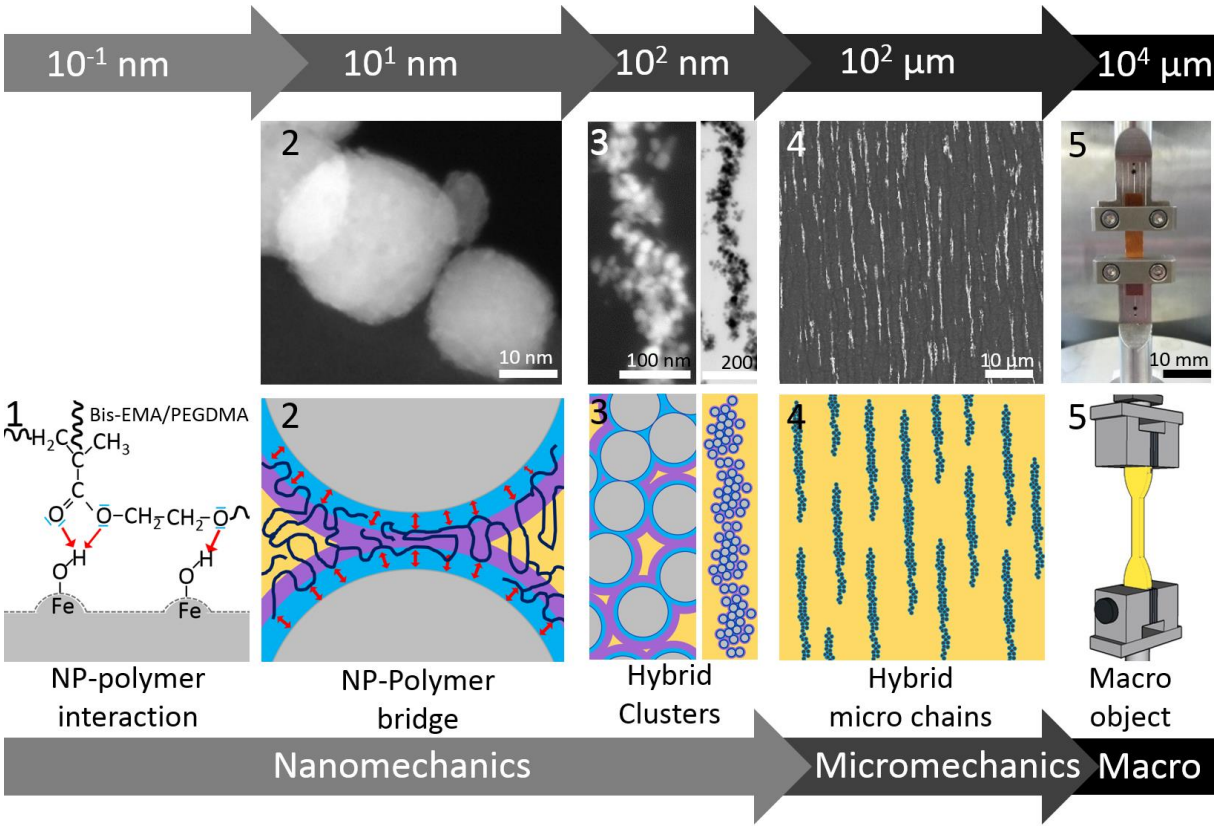

Figure 13 Model of magnetically assembled polymer nanocomposite with a multi-level hierarchy (bottom panel of the images) and the images of structural features at various levels (upper panel of the images). Arrows indicate a bottom-up formation of the material and the length scale of individual levels. Detailed description of the multi-level hierarchy is provided in following text bellow.

Multi-level hierarchy from nano to macro:
Level 1: Molecular level interaction and anchoring of polar groups in backbone of polymer chains with hydroxyl groups on the surface of inorganic nanoparticles.
Level 2: Adsorption of polymer chains due to molecular interaction with NP surface and confinement of polymer chains between close NPs resulting in different relaxation time compared to bulk matrix. Creation of layer of strongly adsorbed (blue) and much looser (purple) bounded segments creating diffuse layer gradually diminishing into bulk unaffected polymer (yellow).
Level 3: Percolation of NPs by direct NP-NP contacts and clustering via polymer segments creating the NP-polymer bridge. Here the interparticle interactions, deformation of polymer bridges plays pivotal role in stiffness of structure.
Level 4: Anisotropic hybrid micro superstructures with specific orientation and spatial arrangement distributed in bulk polymer matrix. Here, the continuum micromechanics models may be applied. The stiffness of the particle structure and surrounding matrix is E_F and E_M, respectively.
Level 5: Macroscopic object with a multi-level hierarchy.

Non-zero stiffness of NP-NP interaction might be an interesting concept, but stiffness of these interactions needs to be on the order of stiffness of surrounding medium to be reinforcing effective. It is assumed that stiffness of particle structure and strength of van der Waals attraction is frequency independent in common frequency ranges (*87*) and presumably also temperature independent (or much negligibly compared to polymers). Also, magnetic

interactions are expected to become stronger with decreasing temperature and thus significantly contributes to PNC's stiffness at low temperatures. This makes interpretation of temperature dependency of reinforcing ratio via interparticle forces quite hard. And if these NP-NP interactions contribute to mechanical robustness of PNCs in some way, their effect will be strongest mainly in rubbery region. Despite, mechanical properties of particle aggregates exhibit some elastic features and non-zero stiffness (*46-52*), only stiffness of NP-NP bonds itself cannot explain the viscoelastic behaviour and disappearance of the reinforcement effect in PNCs close to their T_g. This feature is general for all PNCs using matrices of various mechanical properties. Same effect of the temperature on the reinforcement of PNCs is observed in this work. This means that forces which support the load carrying capability of the structures depend on the actual stiffness of surrounding medium and bound polymer layers and their vitrification characteristics.

The contribution of bound layer and particle deformation is discussed further in text. Theory for orientation and temperature dependent reinforcement of magnetically structured PNCs from rubber to glass is schematically depicted in Figure 14B and described in following text. Author believes that this mechanism can be used for description of the temperature dependent reinforcing effectivity in PNCs by a slight modification depending on the geometry of the particle assemblies varying from system to system.

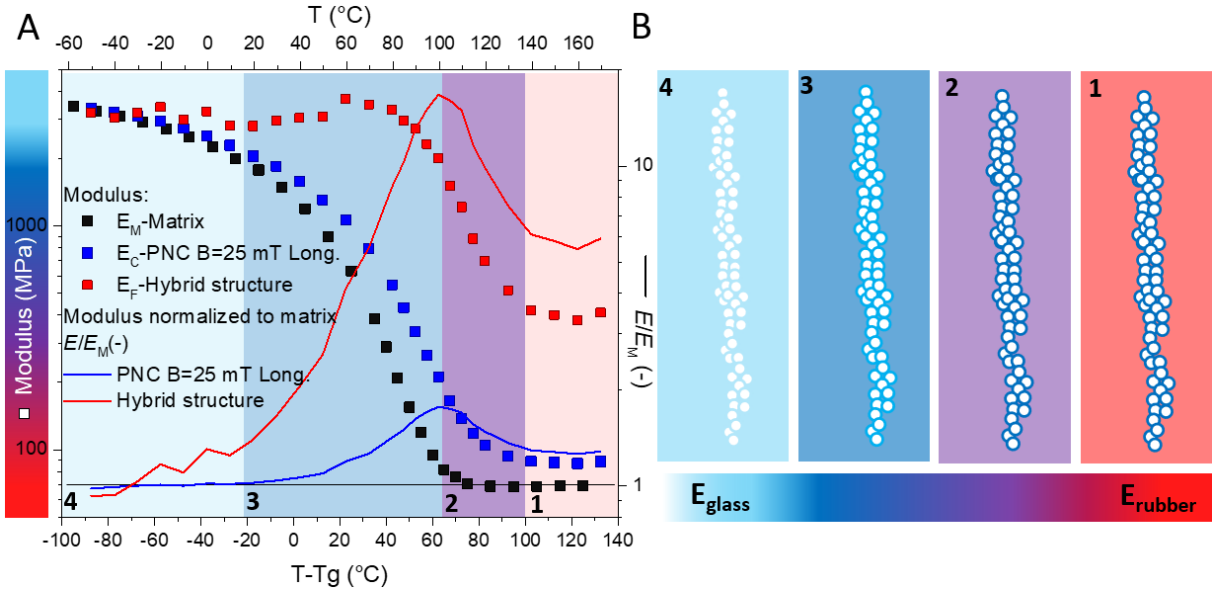

Figure 14 (A) Left *y*-axis – Dependency of calculated stiffness of hybrid structure (E_F) with modulus of neat matrix and PNC assembled in B=25 mT (square symbols □). Right *y*-axis – Relative ratio between stiffness of hybrid structure and its PNC normalized to matrix modulus (solid lines ─). (B) Schematic depiction of vitrification process from rubbery through transition to glassy region. Color bar indicates a stiffness of individual components – hybrid fibers and surrounding matrix. White color represents a stiffness of magnetite particles (~175 GPa).

Region 1 – Rubber

Immobilized polymer segments bridge MNPs clusters also in rubbery state of bulk matrix and give a rise to the stiffness of micro- and macroscopically percolated hybrid nanostructures. The stiffness of hybrid structure calculated using micromechanical models fairly aggress with this idea. The value of hybrid structure is one order of magnitude higher than modulus of neat rubbery matrix, see Figure 14A. The stress from the matrix is carried by the hybrid structure, due to large mismatch of their moduli, $E_F > E_M$ with 6-times higher stiffness than matrix. Also, structure orientation and its length play a role, thus self-assembled and transversely oriented

systems are far less successful in system reinforcement and consequently they exhibit only small reinforcing peak (Figure 11D) on contrary to longitudinal orientations.

Region 2 – Increase of reinforcing ratio

This region is relatively narrow however, the most intense reinforcement of PNC occurs mainly here. During cooling, storage modulus of PNC starts to upturn rapidly bellow ~140 °C while stiffness of matrix remains almost constant for longer period of temperatures, see Figure 14A. As temperature decreases, strongly adsorbed and confined polymer segments in the nearness of NPs vitrify as first and bound the whole hybrid structure by stiff polymer layer with a stiffness far exceeding the properties of bulk matrix which still remain in rubbery state ($E_F >> E_M$). At the end of this region, matrix's modulus starts to upturn as well, and it will slowly catch-up with a hybrid structure. In the addition to large mismatch between E_F and E_M, enhanced stiffness on the interface between bulky matrix and hybrid structure might be beneficial for loading the structures. With an increasing load, polymer bridges may experience much extensive strain amplification which may contribute to stiffness of structures as well.

Region 3 – Decrease of reinforcing ratio

In this region bulk matrix is progressively vitrified and its modulus catch-up with the hybrid structure. Matrix stiffness is gradually increasing and mismatch between E_F and E_M is slowly vanishing ($E_F > E_M$). As their ratio becomes smaller and smaller, micromechanical stress transfer is also more ineffective and less load is carried by hybrid structures. Hybrid structure reach its maximum vitrification degree at much higher temperatures when compared to neat matrix, see Figure 14A. Note that, maximum modulus of vitrified glassy structure is comparable with the modulus of matrix modulus far bellow T_g, such as $T = T_g$-100 °C. From this point, only matrix vitrifies and slowly wipes off the mismatch between moduli.

Region 4 – Glass

Since hybrid structure is already vitrified, only bulk matrix vitrifies with a vanishing of mismatch between their moduli around glass transition. Both phases are thus more or less the same glass ($E_F \approx E_M$) and reinforcement of PNCs modulus by the addition of NPs can be described by deformation of atomistic structure of filler phase – volume replacement. Discrepancies and shifting of modulus along *y*-axis may be attributed to significant confinement, anisotropic coil shapes, or enormous physico-chemical cross-linking with NPs.

4 Conclusion

In contrary to self-assembly of nanoparticle, magnetic directed self-assembly method offers a possibility to control the morphology of particles assemblies, their orientation and anisotropy in bottom-up manner.

Self-assembled systems exhibit relatively large particle aggregates formed by complex bottom-up aggregation process. The effect of the magnetic interactions ensured by non-zero magnetic moment of dipoles was studied to describe the aggregation nature of MNPs. Calculations of van der Waals and magnetic attraction exhibit the regions where particles are close enough to be magnetically attracted across relatively large distances. The addition of only 1 vol. % of MNPs with sufficiently strong magnetic moment was shown to cause aggregation of MNPs into complex shapes even in absence of the external magnetic field.

The application of magnetic field of various strengths resulted in controlled structuring of magnetic material in polymer matrix into anisotropic one-dimensional particle chains. The kinetics of assembling process in magnetic field was studied. It is shown that structure in low magnetic field (B=5 mT) are slowly deposited along the field direction however, the growth of the building-blocks maintains self-assembly nature. Also, fractal-like aggregates with an anisotropy and percolation on the micro length scales were fabricated in PNCs filled with 2 vol. % of MNPs. The application of higher magnetic fields (B=25 and 50 mT) led to rapid arrangement of particles and their self-assembled aggregates into high aspect ratio structures homogeneously oriented within the polymeric material. While, relatively small microchains were created after short assembling times (t_a=10 sec.), structures assembled after longer times gradually transform to large microscopic fibers. It has been shown that the controlling of assembling process by the strength of external field, particle volume fraction, viscosity of medium and assembling time leads to variety of magnetic structures which may find their usage in PNCs technology and/or fundamental types of studies.

Mechanical response of magnetically structured PNCs exhibits significant anisotropy for longitudinally and transversely oriented structures. On the other hand, reinforcement of polymer matrix was observed only above the glass transition of matrix which is classic signature of PNCs. Reinforcement effect of particle structures in the polymer matrix exhibits significant temperature dependence with a maximum in the temperature region around T_g+60°C. Longitudinally oriented structures exhibit considerably larger reinforcing capability. Anisotropy of PNCs systems was described by the different load carrying capability which is higher for longitudinally oriented structures while transversely oriented structures contribute only negligibly to mechanical robustness on PNC. The structure of magnetically assembled PNCs on the different length scales was analysed by hierarchic model of material with various contributions of individual levels of material to mechanical properties. At the micro scale level, approximation of anisotropic particle structures by solid hybrid fibers with a non-zero stiffness was utilized in the combination with a micromechanics model for composite system. Temperature dependent stiffness of hybrid structures was calculated using Halpin-Tsai model exhibiting much higher stiffness than surrounding matrix. The intrinsic stiffness of magnetically structures were attributed to vitrification of polymer segments in the vicinity and confined by MNPs. These polymer segments penetrate thorough the particle structures and transmit the stress. The presence of polymer bridge with sufficiently high molecular weight and stiffness is absolutely essential for the mechanical robustness of PNCs. Proposed theory of reinforcement can be generally applied for all PNCs creating nano-, submicro-, micro- and macro particle structures. In cases studied here, anisotropic micro particle structures are created by magnetic guidance.

References

1. L. He, M. Wang, J. Ge, Y. Yin, Magnetic Assembly Route to Colloidal Responsive Photonic Nanostructures. *Accounts of Chemical Research* 45, 1431-1440 (2012).
2. J. J. Weis, Simulation of quasi-two-dimensional dipolar systems. *J. Phys.-Condes. Matter* 15, S1471-S1495 (2003).
3. J. J. Weis, Low density quasi-two-dimensional dipolar hard spheres in an external field. *Mol. Phys.* 103, 7-10 (2005).
4. J. Richardi, M. P. Pileni, J. J. Weis, Self-organization of magnetic nanoparticles: A Monte Carlo study. *Physical Review E* 77, 9 (2008).
5. J. Richardi, M. P. Pileni, J. J. Weis, Self-organization of confined dipolar particles in a parallel field. *Journal of Chemical Physics* 130, 6 (2009).
6. C. Salzemann, J. Richardi, I. Lisiecki, J. J. Weis, M. P. Pileni, Mesoscopic Void Structures in Cobalt Nanocrystal Films Formed from Drying Concentrated Colloidal Solutions. *Physical Review Letters* 102, 4 (2009).
7. J. W. Swan, J. L. Bauer, Y. F. Liu, E. M. Furst, Directed colloidal self-assembly in toggled magnetic fields. *Soft Matter* 10, 1102-1109 (2014).
8. A. P. Hynninen, M. Dijkstra, Phase diagram of dipolar hard and soft spheres: Manipulation of colloidal crystal structures by an external field. *Physical Review Letters* 94, 4 (2005).
9. L. Ye, T. Pearson, Y. Cordeau, O. T. Mefford, T. M. Crawford, Triggered self-assembly of magnetic nanoparticles. *Scientific Reports* 6, 9 (2016).
10. J. J. Weis, Orientational structure of quasi-two-dimensional dipolar hard spheres. *Mol. Phys.* 93, 361-364 (1998).
11. J. Richardi, J. J. Weis, Low density mesostructures of confined dipolar particles in an external field. *Journal of Chemical Physics* 135, 10 (2011).
12. J. Richardi, J. J. Weis, Influence of short range potential on field induced chain aggregation in low density dipolar particles. *Journal of Chemical Physics* 138, 4 (2013).
13. J. Jestin *et al.*, Anisotropic reinforcement of nanocomposites tuned by magnetic orientation of the filler network. *Advanced Materials* 20, 2533-+ (2008).
14. D. Fragouli *et al.*, Dynamical Formation of Spatially Localized Arrays of Aligned Nanowires in Plastic Films with Magnetic Anisotropy. *Acs Nano* 4, 1873-1878 (2010).
15. A. S. Robbes *et al.*, Nanocomposite Materials with Controlled Anisotropic Reinforcement Triggered by Magnetic Self-Assembly. *Macromolecules* 44, 8858-8865 (2011).
16. K. E. Roskov, J. E. Atkinson, L. M. Bronstein, R. J. Spontak, Magnetic field-induced alignment of nanoparticles in electrospun microfibers. *Rsc Advances* 2, 4603-4607 (2012).
17. H. Y. Yuan *et al.*, Facile Assembly of Aligned Magnetic Nanoparticle Chains in Polymer Nanocomposite Films by Magnetic Flow Coating. *Acs Applied Materials & Interfaces* 9, 11290-11298 (2017).
18. Z. Rigbi, J. E. Mark, EFFECTS OF A MAGNETIC-FIELD APPLIED DURING THE CURING OF A POLYMER LOADED WITH MAGNETIC FILLER. *Journal of Polymer Science Part B-Polymer Physics* 23, 1267-1269 (1985).
19. G. B. Sohoni, J. E. Mark, ANISOTROPIC REINFORCEMENT IN ELASTOMERS CONTAINING MAGNETIC FILLER PARTICLES. *Journal of Applied Polymer Science* 34, 2853-2859 (1987).
20. C. Bellan, G. Bossis, Field dependence of viscoelastic properties of MR elastomers. *International Journal of Modern Physics B* 16, 2447-2453 (2002).

21. F. Xu *et al.*, Three-Dimensional Magnetic Assembly of Microscale Hydrogels. *Advanced Materials* 23, 4254-4260 (2011).
22. D. Lorenzo *et al.*, Formation and magnetic manipulation of periodically aligned microchains in thin plastic membranes. *Journal of Applied Physics* 112, (2012).
23. P. Song *et al.*, Mechanical properties of silicone composites reinforced with micron- and nano-sized magnetic particles. *Express Polymer Letters* 7, 546-553 (2013).
24. P. J. Krommenhoek, J. B. Tracy, Magnetic Field-Directed Self-Assembly of Magnetic Nanoparticle Chains in Bulk Polymers. *Particle & Particle Systems Characterization* 30, 759-763 (2013).
25. S. R. Mishra, M. D. Dickey, O. D. Velev, J. B. Tracy, Selective and directional actuation of elastomer films using chained magnetic nanoparticles. *Nanoscale* 8, 1309-1313 (2016).
26. S. Marchi, A. Casu, F. Bertora, A. Athanassiou, D. Fragouli, Highly Magneto-Responsive Elastomeric Films Created by a Two-Step Fabrication Process. *Acs Applied Materials & Interfaces* 7, 19112-19118 (2015).
27. C. Hintze *et al.*, Soft magnetic Elastomers with controllable Stiffness: Experiments and Modelling. *Kgk-Kautschuk Gummi Kunststoffe* 67, 53-59 (2014).
28. D. Le Roy *et al.*, Anisotropic ferromagnetic polymer: A first step for their implementation in microfluidic systems. *AIP Adv.* 6, 6 (2016).
29. J. P. Ge *et al.*, Magnetochromatic Microspheres: Rotating Photonic Crystals. *Journal of the American Chemical Society* 131, 15687-15694 (2009).
30. D. Fragouli *et al.*, Nanocomposite Pattern-Mediated Magnetic Interactions for Localized Deposition of Nanomaterials. *Acs Applied Materials & Interfaces* 5, 7253-7257 (2013).
31. C. Peters *et al.*, Visible Light Curing of Epon SU-8 Based Superparamagnetic Polymer Composites with Random and Ordered Particle Configurations. *Acs Applied Materials & Interfaces* 7, 193-200 (2015).
32. J. Jancar, Review of the role of the interphase in the control of composite performance on micro- and nano-length scales. *Journal of Materials Science* 43, 6747-6757 (2008).
33. J. Jancar *et al.*, Current issues in research on structure-property relationships in polymer nanocomposites. *Polymer* 51, 3321-3343 (2010).
34. J. Kalfus, J. Jancar, Relaxation processes in PVAc-HA nanocomposites. *Journal of Polymer Science Part B-Polymer Physics* 45, 1380-1388 (2007).
35. J. Kalfus, J. Jancar, Immobilization of polyvinylacetate macromolecules on hydroxyapatite nanoparticles. *Polymer* 48, 3935-3937 (2007).
36. J. Kalfus, J. Jancar, Elastic response of nanocomposite poly(vinylacetate)-hydroxyapatite with varying particle shape. *Polymer Composites* 28, 365-371 (2007).
37. J. Kalfus, J. Jancar, Viscoelastic response of nanocomposite poly(vinyl acetate)-hydroxyapatite with varying particle shape-dynamic strain softening and modulus recovery. *Polymer Composites* 28, 743-747 (2007).
38. J. Jancar, L. Recman, Particle size dependence of the elastic modulus of particulate filled PMMA near its T-g. *Polymer* 51, 3826-3828 (2010).
39. J. Jancar, R. S. Hoy, A. J. Lesser, E. Jancarova, J. Zidek, Effect of Particle Size, Temperature, and Deformation Rate on the Plastic Flow and Strain Hardening Response of PMMA Composites. *Macromolecules* 46, 9409-9426 (2013).
40. J. Jancar, R. S. Hoy, E. Jancarova, J. Zidek, Effect of temperature, strain rate and particle size on the yield stresses and post-yield strain softening of PMMA and its composites. *Polymer* 63, 196-207 (2015).

41. N. Jouault *et al.*, Well-Dispersed Fractal Aggregates as Filler in Polymer-Silica Nanocomposites: Long-Range Effects in Rheology. *Macromolecules* 42, 2031-2040 (2009).
42. N. Jouault, F. Dalmas, F. Boue, J. Jestin, Multiscale characterization of filler dispersion and origins of mechanical reinforcement in model nanocomposites. *Polymer* 53, 761-775 (2012).
43. J. F. Moll *et al.*, Mechanical Reinforcement in Polymer Melts Filled with Polymer Grafted Nanoparticles. *Macromolecules* 44, 7473-7477 (2011).
44. J. Oberdisse, Aggregation of colloidal nanoparticles in polymer matrices. *Soft Matter* 2, 29-36 (2006).
45. T. A. Witten, M. Rubinstein, R. H. Colby, REINFORCEMENT OF RUBBER BY FRACTAL AGGREGATES. *Journal De Physique Ii* 3, 367-383 (1993).
46. S. K. Friedlander, K. Ogawa, M. Ullmann, Elastic behavior of nanoparticle chain aggregates: A hypothesis for polymer-filler behavior. *Journal of Polymer Science Part B-Polymer Physics* 38, 2658-2665 (2000).
47. Y. J. Suh, S. V. Prikhodko, S. K. Friedlander, Nanostructure manipulation device for transmission electron microscopy: application to titania nanoparticle chain aggregates. *Microsc. microanal.* 8, 497-501 (2002).
48. Y. J. Suh, S. K. Friedlander, Origins of the elastic behavior of nanoparticle chain aggregates: Measurements using nanostructure manipulation device. *Journal of Applied Physics* 93, 3515-3523 (2003).
49. W. Z. Rong, A. E. Pelling, A. Ryan, J. K. Gimzewski, S. K. Friedlander, Complementary TEM and AFM force spectroscopy to characterize the nanomechanical properties of nanoparticle chain aggregates. *Nano Letters* 4, 2287-2292 (2004).
50. R. Bandyopadhyaya, W. Z. Rong, S. K. Friedlander, Dynamics of chain aggregates of carbon nanoparticles in isolation and in polymer films: Implications for nanocomposite materials. *Chemistry of Materials* 16, 3147-3154 (2004).
51. A. Dalis, S. K. Friedlander, Molecular dynamics simulations of the straining of nanoparticle chain aggregates: the case of copper. *Nanotechnology* 16, S626-S631 (2005).
52. W. Z. Rong, W. Q. Ding, L. Madler, R. S. Ruoff, S. K. Friedlander, Mechanical properties of nanoparticle chain aggregates by combined AFM and SEM: Isolated aggregates and networks. *Nano Letters* 6, 2646-2655 (2006).
53. P. S. Antonel *et al.*, Magnetic and elastic properties of CoFe2O4- polydimethylsiloxane magnetically oriented elastomer nanocomposites. *Journal of Applied Physics* 110, 8 (2011).
54. K. Keshoju, L. Sun, Mechanical characterization of magnetic nanowire-polydimethylsiloxane composites. *Journal of Applied Physics* 105, 5 (2009).
55. K. Ikemura, K. Ichizawa, M. Yoshida, S. Ito, T. Endo, UV-VIS spectra and photoinitiation behaviors of acylphosphine oxide and bisacylphosphine oxide derivatives in unfilled, light-cured dental resins. *Dent. Mater. J.* 27, 765-774 (2008).
56. T. Nardi *et al.*, UV-cured transparent magnetic polymer nanocomposites. *Polymer* 54, 4472-4479 (2013).
57. V. Melinte *et al.*, Preparation and properties of photopolymerized hybrid composites with covalently attached magnetite nanoparticles. *Chemical Engineering Journal* 259, 542-551 (2015).
58. Y. Lalatonne, J. Richardi, M. P. Pileni, Van der Waals versus dipolar forces controlling mesoscopic organizations of magnetic nanocrystals. *Nature Materials* 3, 121-125 (2004).

59. C. Xu, K. Ohno, V. Ladmiral, R. J. Composto, Dispersion of polymer-grafted magnetic nanoparticles in homopolymers and block copolymers. *Polymer* 49, 3568-3577 (2008).
60. A. S. Robbes *et al.*, Homogeneous Dispersion of Magnetic Nanoparticles Aggregates in a PS Nanocomposite: Highly Reproducible Hierarchical Structure Tuned by the Nanoparticles' Size. *Macromolecules* 43, 5785-5796 (2010).
61. Y. Jiao, P. Akcora, Assembly of Polymer-Grafted Magnetic Nanoparticles in Polymer Melts. *Macromolecules* 45, 3463-3470 (2012).
62. S. Sierra-Bermudez, L. P. Maldonado-Camargo, F. Orange, M. J. F. Guinel, C. Rinaldi, Assessing magnetic nanoparticle aggregation in polymer melts by dynamic magnetic susceptibility measurements. *J. Magn. Magn. Mater.* 378, 64-72 (2015).
63. M. Ashjari, A. R. Mahdavian, N. G. Ebrahimi, Y. Mosleh, Efficient Dispersion of Magnetite Nanoparticles in the Polyurethane Matrix Through Solution Mixing and Investigation of the Nanocomposite Properties. *J. Inorg. Organomet. Polym. Mater.* 20, 213-219 (2010).
64. B. Bharti, A. L. Fameau, M. Rubinstein, O. D. Velev, Nanocapillarity-mediated magnetic assembly of nanoparticles into ultraflexible filaments and reconfigurable networks. *Nature Materials* 14, 1104-+ (2015).
65. J. H. E. Promislow, A. P. Gast, Magnetorheological fluid structure in a pulsed magnetic field. *Langmuir* 12, 4095-4102 (1996).
66. S. A. Majetich, M. Sachan, Magnetostatic interactions in magnetic nanoparticle assemblies: energy, time and length scales. *Journal of Physics D-Applied Physics* 39, R407-R422 (2006).
67. S. E. Kushnir, P. E. Kazin, L. A. Trusov, Y. D. Tretyakov, Self-organization of micro- and nanoparticles in ferrofluids. *Russian Chemical Reviews* 81, 560-570 (2012).
68. J. Zidek, J. Kucera, J. Jancar, Nearest Particle Distance and the Statistical Distribution of Agglomerates from a Model of a Finite Set of Particles. *Cmc-Computers Materials & Continua* 24, 183-208 (2011).
69. J. Zidek, Personal Discussion. (2018).
70. Z. Varga, G. Filipcsei, M. Zrinyi, Magnetic field sensitive functional elastomers with tuneable elastic modulus. *Polymer* 47, 227-233 (2006).
71. J. L. Mietta *et al.*, Anisotropic Magnetoresistance and Piezoresistivity in Structured Fe3O4-Silver Particles in PDMS Elastomers at Room Temperature. *Langmuir* 28, 6985-6996 (2012).
72. R. A. Landa *et al.*, Magnetic and elastic anisotropy in magnetorheological elastomers using nickel-based nanoparticles and nanochains. *Journal of Applied Physics* 114, 11 (2013).
73. Y. Han, W. Hong, L. A. E. Faidley, Field-stiffening effect of magneto-rheological elastomers. *Int. J. Solids Struct.* 50, 2281-2288 (2013).
74. Y. H. Song, Q. Zheng, Concepts and conflicts in nanoparticles reinforcement to polymers beyond hydrodynamics. *Progress in Materials Science* 84, 1-58 (2016).
75. K. W. Putz, M. J. Palmeri, R. B. Cohn, R. Andrews, L. C. Brinson, Effect of cross-link density on interphase creation in polymer nanocomposites. *Macromolecules* 41, 6752-6756 (2008).
76. Y. Zare, H. Garmabi, Analysis of Tensile Modulus of PP/Nanoclay/CaCO3 Ternary Nanocomposite Using Composite Theories. *Journal of Applied Polymer Science* 123, 2309-2319 (2012).
77. E. Guth, THEORY OF FILLER REINFORCEMENT. *Journal of Applied Physics* 16, 20-25 (1945).
78. H. M. Smallwood, Limiting Law of the Reinforcement of Rubber. *Journal of Applied Physics* 15, 758-766 (1944).

79. P. Sotta *et al.*, Nonentropic Reinforcement in Elastomer Nanocomposites. *Macromolecules* 50, 6314-6322 (2017).
80. F. Lu, H. H. Kausch, W. J. Cantwell, M. Fischer, The effect of crosslink density on the fracture toughness of core-shell modified epoxy resins. *J. Mater. Sci. Lett.* 15, 1018-1021 (1996).
81. J. Jancar, The Thickness Dependence of Elastic Modulus of Organosilane Interphases. *Polymer Composites* 29, 1372-1377 (2008).
82. H. Mortazavian, C. J. Fennell, F. D. Blum, Structure of the Interfacial Region in Adsorbed Poly(vinyl acetate) on Silica. *Macromolecules* 49, 298-307 (2016).
83. N. Jouault *et al.*, Bound Polymer Layer in Nanocomposites. *Acs Macro Letters* 2, 371-374 (2013).
84. S. E. Harton *et al.*, Immobilized Polymer Layers on Spherical Nanoparticles. *Macromolecules* 43, 3415-3421 (2010).
85. S. W. Cheng *et al.*, Interfacial Properties of Polymer Nanocomposites: Role of Chain Rigidity and Dynamic Heterogeneity Length Scale. *Macromolecules* 50, 2397-2406 (2017).
86. C. Housmans, M. Sferrazza, S. Napolitano, Kinetics of Irreversible Chain Adsorption. *Macromolecules* 47, 3390-3393 (2014).
87. H. L. Xu, Y. H. Song, Q. X. Zhang, Q. Zheng, Contributions of silica network and interfacial fraction in reinforcement and Payne effect of polypropylene glycol nanocomposites. *Polymer* 138, 139-145 (2018).
88. S. Y. Kim, C. F. Zukoski, Molecular Weight Effects on Particle and Polymer Microstructure in Concentrated Polymer Solutions. *Macromolecules* 46, 6634-6643 (2013).
89. B. J. Anderson, C. F. Zukoski, Rheology and Microstructure of an Unentangled Polymer Nanocomposite Melt. *Macromolecules* 41, 9326-9334 (2008).
90. H. Mortazavian, C. J. Fennell, F. D. Blum, Surface Bonding Is Stronger for Poly(methyl methacrylate) than for Poly(vinyl acetate). *Macromolecules* 49, 4211-4219 (2016).
91. J. Moll, S. K. Kumar, Glass Transitions in Highly Attractive Highly Filled Polymer Nanocomposites. *Macromolecules* 45, 1131-1135 (2012).
92. Q. Chen *et al.*, Mechanical Reinforcement of Polymer Nanocomposites from Percolation of a Nanoparticle Network. *Acs Macro Letters* 4, 398-402 (2015).
93. A. N. Rissanou *et al.*, Structural and Conformational Properties of Poly(ethylene oxide)/Silica Nanocomposites: Effect of Confinement. *Macromolecules* 50, 6273-6284 (2017).
94. U. G. K. Wegst, H. Bai, E. Saiz, A. P. Tomsia, R. O. Ritchie, Bioinspired structural materials. *Nature Materials* 14, 23-36 (2015).
95. G. Chen *et al.*, Mechanical and dynamic properties of resin blend and composite systems: A molecular dynamics study. *Composite Structures* 190, 160-168 (2018).
96. J. S. Meth, S. R. Lustig, Polymer interphase structure near nanoscale inclusions: Comparison between random walk theory and experiment. *Polymer* 51, 4259-4266 (2010).
97. A. Mujtaba *et al.*, Detection of Surface-Immobilized Components and Their Role in Viscoelastic Reinforcement of Rubber-Silica Nanocomposites. *Acs Macro Letters* 3, 481-485 (2014).
98. J. Berriot, H. Montes, F. Lequeux, D. Long, P. Sotta, Evidence for the shift of the glass transition near the particles in silica-filled elastomers. *Macromolecules* 35, 9756-9762 (2002).

99. M. Tauban, J. Y. Delannoy, P. Sotta, D. R. Long, Effect of Filler Morphology and Distribution State on the Linear and Nonlinear Mechanical Behavior of Nanofilled Elastomers. *Macromolecules* 50, 6369-6384 (2017).
100. J. Berriot *et al.*, Filler-elastomer interaction in model filled rubbers, a H-1 NMR study. *J. Non-Cryst. Solids* 307, 719-724 (2002).
101. H. Montes, F. Lequeux, J. Berriot, Influence of the glass transition temperature gradient on the nonlinear viscoelastic behavior in reinforced elastomers. *Macromolecules* 36, 8107-8118 (2003).
102. S. Merabia, P. Sotta, D. R. Long, A Microscopic Model for the Reinforcement and the Nonlinear Behavior of Filled Elastomers and Thermoplastic Elastomers (Payne and Mullins Effects). *Macromolecules* 41, 8252-8266 (2008).
103. B. Bar-On, H. D. Wagner, Structural motifs and elastic properties of hierarchical biological tissues - A review. *J. Struct. Biol.* 183, 149-164 (2013).
104. B. Bar-On, H. D. Wagner, The emergence of an unusual stiffness profile in hierarchical biological tissues. *Acta Biomater.* 9, 8099-8109 (2013).
105. B. Bar-On, H. D. Wagner, New insights into the Young's modulus of staggered biological composites. *Mater. Sci. Eng. C-Mater. Biol. Appl.* 33, 603-607 (2013).
106. J. C. Halpin Affdl, J. L. Kardos, The Halpin-Tsai equations: A review. 16, 344–352 (1976).
107. R. Hentschke, J. Hager, N. W. Hojdis, Molecular Modeling Approach to the Prediction of Mechanical Properties of Silica-Reinforced Rubbers. *Journal of Applied Polymer Science* 131, 9 (2014).
108. J. Hager, R. Hentschke, N. W. Hojdis, H. A. Karimi-Varzaneh, Computer Simulation of Particle-Particle Interaction in a Model Polymer Nanocomposite. *Macromolecules* 48, 9039-9049 (2015).
109. J. Meyer, R. Hentschke, J. Hager, N. W. Hojdis, H. A. Karimi-Varzaneh, Molecular Simulation of Viscous Dissipation due to Cyclic Deformation of a Silica-Silica Contact in Filled Rubber. *Macromolecules* 50, 6679-6689 (2017).

Author's publications and other outputs

Scientific conferences:
CEITEC PhD retreat, Valtice, 2015 – Active participant with a poster and abstract in book of abstracts: *Short fiber reinforced thermoplastic composites*
Chemistry & Life 2015, Brno, 2015 – Active participant with a poster, abstract in book of abstracts and article in conference proceeding book: *Force-assembled Fe_3O_4 particle chains in polyurethane matrix*
Creating Life in 3D, Brno, 2015 - Active participant with a poster: *Force-assembled Fe_3O_4 particle chains in polyurethane matrix*
Structure and Dynamics of Polymer Nanocomposites, Montpellier, 2015, – Active participant with a presentation and abstract in book of abstracts: *Magnetic force-assembled polymer nanocomposites*
CEITEC PhD retreat 2, Telc, 2017 – Active participant with a poster and abstract in book of abstracts: *Magnetic field directed self-assembly as route for biomimetics*
Deformation, yield and fracture of polymers, Rolduc, 2018 – Active participant with a poster and abstract in book of abstracts: *Mechanical anisotropy induced by magnetically assembled particle fibrous assemblies in photopolymer matrix*

Research projects:
Magnetic field directed self-assembly as route for bottom-up build-up approach inspired by nature – research team leader
Control of nanoparticle self-assembly in polymer liquids and effect of nanostructure on the thermo-mechanical properties of resulted nanocomposites – member of research team
Nízkohustotní funkční nanokompozity (GAČR) – research team member
Výzkum odpadních termoplastů (TAČR) – research team member
Mechanismy a kinetika samouspořádávání nanočástic v hierarchických polymerních kompozitech (GAČR) – research team member

Publications:
Zboncak, M.; Ondreas, F.; Jancar, J. Force-Assembled Fe_3O_4 Particle Chains in Polyurethane Matrix. *Materials Science Forum,* 221-225 (2016).
P. Lepcio, F. Ondreas, K. Zarybnicka, M. Zboncak, O. Caha, J. Jancar, Bulk polymer nanocomposites with preparation protocol governed nanostructure: the origin and properties of aggregates and polymer bound clusters. *Soft Matter* 14, 2094-2103 (2018).
M. Zboncak, J. Jancar, Toughening of PMMA by short poly(p-phenylene-2,6-benzobisoxazole) fibers. *Express Polymer Letters* 12, 753-766 (2018).

Internships:
TU Wien, Institute of Materials Science and Technology – Research group of Jürgen Stampfl
Weizmann Institute of Science, Materials and Interfaces – Research group of Daniel H. Wagner

Pedagogical experience:
Participation on the teaching of the course Composite materials and their technologies II